# *Reviews*

## Ordered Mesoporous Materials for Bioadsorption and Biocatalysis

Martin Hartmann*

*Department of Chemistry, Chemical Technology, TU Kaiserslautern, P.O. Box 3049, D-67653, Kaiserslautern, Germany*

*Received August 27, 2004. Revised Manuscript Received May 27, 2005*

The encapsulation of enzymes and other proteins into inorganic host materials has attracted considerable attention over the past few years. This research has demonstrated that biomolecules immobilized in inorganic matrixes retain their functional characteristics to a large extent. These new materials are of interest for applications as (optically based) biosensors and biocatalysts. We review the growing field of amino acids, vitamins, enzymes, and whole cells adsorbed (immobilized) onto ordered mesoporous silica and carbon molecular sieves. Strategies for the preparation of mesoporous supports and the essential properties of the resulting materials with respect to the envisaged applications are presented. Basic effects of the nature of the adsorption and various aspects of the application of these materials as biosensors, bicatalysts, and for drug release are discussed. Outlook of potential applications and further challenges are also provided.

### 1. Introduction

The adsorption of proteins from solution onto solid surfaces has attracted much attention due to its scientific importance and application in many areas.[1−3] In medical and food industries, it is essential to remove adsorbed proteins since even a small amount of deposited proteins may give rise to the subsequent adsorption of fibrous proteins leading to adverse biological consequences.[4−6] Protein adsorption can also contribute to blood clotting and heart disease.[7] The adsorption (immobilization) of proteins on inorganic materials is crucial because of the potential to improve the stability of enzymes under extreme conditions.[8] The controlled adsorption of proteins is essential in the fields of enzymatic catalysis, biosensors, and disease diagnostics.[9−11]

Adsorption of proteins over controlled porous glass (CPG) and sol−gels has been extensively studied for possible applications as biosensors[12,13] and reviewed by Weetall[14] and Avnir,[15] respectively. The recent advances in the entrapment of proteins and other biological species into a wide range of sol−gel-derived nanocomposite materials and their use for biosensor and biological applications have been reviewed by Gill[16] and Jin and Brennan.[17] The major disadvantage of CPG materials for adsorption studies are their high cost and more importantly their surface area, which rapidly decreases with increasing pore size (30−200 nm).[13] The discovery of mesoporous silicate molecular sieves opened up new possibilities in many areas of chemistry and material science.[18−21] These materials possess high specific surface areas, high specific pore volumes, and well-ordered pore structures with uniform mesopores adjustable in diameter from about 1.5 to 30 nm. Mesoporous materials have a clear advantage over microporous zeolites and zeotype molecular sieves for the adsorption and transformation of large organic molecules.[22,23]

The materials described below are mainly mesoporous inorganic hosts obtained by hydrothermal synthesis and characterized by a regular arrangement of mesopores with a narrow pore size distribution. According to the IUPAC definition, pores with diameters between 2 and 50 nm are termed mesopores. Nowadays, the popular term "nanoporous" materials is often used, which is only loosely defined as materials having pores in the nanometer range.[24] Mesoporous materials are further characterized by high specific surface areas (up to ca. 1500 $m^2/g$) and pore volumes (up to ca. 1.5 $cm^3/g$), which renders them ideal candidates as hosts for biomolecules. Moreover, variation of the synthesis conditions enables the researchers to tailor the inorganic host so that the encapsulation of a variety of proteins, enzymes, and other biological molecules is feasible. The described materials fulfill many of the requirements for enzyme carriers such as large surface area, sufficient functional groups for enzyme attachment, hydrophilic character, water insolubility, chemical and thermal stability, mechanical strength, suitable particle form, regenerability, and toxicological safety.

The observation that some enzymes retain their functionality upon immobilization on ordered mesoporous supports triggered significant research activity in encapsulating enzymes as well as other bioactive components. The rapid growth of this young field calls for an interim summary of the significant volume of activity that has been accumulated so far. The main purpose of this brief review is to provide this outline.

Table 1 shows examples of the variety of biological molecules that have been adsorbed onto ordered mesoporous silica

* To whom correspondence should be addressed. Phone: +49-631-205-3559. Fax: +49-631-205-4193. Email: hartmann@chemie.uni-kl.de.

10.1021/cm0485658 CCC: $30.25 
Published on Web 07/20/2005

**Table 1. Adsorption of Biologically Interesting Compounds on Ordered Mesoporous Materials**

| adsorbate | adsorbent | ref |
|---|---|---|
| | small biological molecules | |
| lysine, phenylalanine, histidine, glutamic acid, asparaginin, etc. | MCM-41 | 44 |
| chorophyll *a* | FSM-16 | 51, 52, 53 |
| vitamin E | CMK-1, CMK-3 | 50 |
| vitamin B2 | MCM-41, MCM-48 | 48 |
| | Purified Proteins | |
| catalase | SBA-15 | 122 |
| conalbumin | SBA-15, thiol-functionalized SBA-15 | 105 |
| conalbumin | APTS-modified MCF | 106 |
| cytochrome *c* | MCM-41, MCM-48, SBA-15, Nb-TMS-1, Nb-TMS-4 | 58, 61, 62 |
| cytochrome *c* | MCM-41, SBA-15 | 63, 64, 65, 66 |
| cyctochrome *c* | SBA-15, thiol-functionalized SBA-15 | 105 |
| cytochrome *c* | MCM-41, SBA-15, AlMCM-41, AlSBA-15 | 67, 68 |
| cytochrome *c* | CMK-3 | 74 |
| HRP | FSM-16, MCM-41, SBA-15 | 93, 94 |
| $\beta$-lactoglobulin | SBA-15, thiol-functionalized SBA-15 | 105 |
| lysozyme | MCM-41, SBA-15 | 48, 82, 83 |
| lysozyme | modified SBA-15 | 84 |
| lysozyme | MCM-41, SBA-15, AlMCM-41, AlSBA-15 | 87 |
| lysozyme | CMK-1, CMK-3 | 90 |
| myoglobin | SBA-15, thiol-functionalized SBA-15 | 105 |
| ovalbumin | SBA-15, thiol-functionalized SBA-15 | 105 |
| papain | MCM-41 | 58 |
| penicilin acylase | MCM-41 | 118 |
| RNase A | MCM-48 | 107 |
| trypsin | MCM-41/SBA-15 | 48, 83 |
| trypsin | SBA-15, thiol-functionalized SBA-15 | 105 |
| trypsin | MCM-41 | 58 |
| trypsin | MCM-41, MCF | 113 |
| subtilisin Carlsberg | FSM-16, MCM-41, SBA-15 | 93, 94 |
| bovine serum albumin | SBA-15, thiol-functionalized SBA-15 | 105 |
| bovine serum albumin | AlMCM-41 | 104 |
| | Whole Cells | |
| *Arthobacter* sp., *Bacillus subtilis*, and *Micrococcus luteus* | MCM-41, AlMCM-41 | 108 |

**Table 2. Properties of Selected Protein Molecules (obtained from protein data bank)**

| protein | molecular weight in solution/Da | molecular dimensions/nm$^3$ | pI |
|---|---|---|---|
| cytochrome *c* | 12 400 | 2.6 × 3.2 × 3.3 | 10.0 |
| lysozyme | 14 388 | 1.9 × 2.5 × 4.3 | 10.8 |
| myoglobin | 17 000 | 2.1 × 3.5 × 4.4 | 7.0 |
| papain | 20 700 | 3.6 | 8.8 |
| trypsin | 23 400 | 3.8 | 10.5 |
| pepsin | 33 000 | n.a | 1.0 |
| $\beta$-lactoglobulin | 35 000 | 2.9 × 3.4 × 4.0 | 5.2 |
| ovalbumin | 43 000 | 4.0 × 5.0 × 7.0 | 4.9 |
| chloroperoxidase | | n.a | 4.1 |
| horseradish peroxidase | 44 000 | 4.0 × 4.4 × 6.8 | 8.8 |
| manganese peroxidase | 45 000 | n.a | 3.6 |
| bovine serum albumin | 66 400 | 5.0 × 7.0 × 7.0 | 4.7 |
| conalbumin | 76 000 | 5.0 × 5.6 × 9.5 | 6.0 |
| glucose oxidase | 160 000 | 7.0 × 5.5 × 8.0 | 4.3 |

and carbon materials. Most adsorbates can either be classified as being proteins or "smaller biological molecules" including amino acids, peptides, and vitamins. The immobilization of whole cells was up until now only reported in one paper.

## 2. Mesoporous Silica and Related Materials

Mesoporous materials are attractive supports for the adsorption or immobilization of biologically relevant molecules in confined spaces in the nanometer range. These supports are generally synthesized through silica polymerization around regularly aligned micelles and subsequent template removal by extraction or calcination (Figure 1). According to the IUPAC classification, materials containing pores with diameters between 2 and 50 are named mesoporous materials. These materials have attracted considerable attention due to their high specific surface area, their large specific pore volume, and narrow pore size distribution, which renders them interesting materials for adsorption and conversion of bulky molecules. In 1990, Kuroda et al.[25] reported the preparation of mesoporous silica with uniform pore size via intercalation of hexadecyclcltrimethylammonium cations into the layered polysilicate kanemite (idealized formula: $NaHSi_2O_3 \cdot 3H_2O$) and subsequent removal of the organic template. These novel materials were named FSM-*n* (Folded Sheet Materials, here *n* is the number of carbon atoms in the surfactant alkyl chain used to synthesize the material). Inagaki et al. reported that the pore diameter of FSM materials can be controlled by varying the alkyl chain length of the cationic surfactant.[26]

The starting point of intensive research in the area of mesoporous materials was the disclosure of the M41S family of silicate/aluminosilicate mesoporous molecular sieves by scientists from Mobil. Here also cationic surfactants possessing alkyl chains from 8 to 22 carbons were used as templates during the hydrothermal synthesis.[18,27] Depending on the shape of the supramolecular template, four different phases have been discovered: a hexagonal phase named MCM-41 (Mobil Composition of Matter No. 41),[18,27] a cubic phase named MCM-48,[28] a lamellar phase MCM-50,[29] and a cubic octamer $[(CTMA)SiO_{2.5}]_8$. MCM-41 possesses honeycomb arrays of nonintersecting uniformly sized channels with diameters ranging from 1.5 to 10 nm depending on the template used, the addition of auxiliary organics, and the synthesis parameters, e.g., synthesis time, synthesis

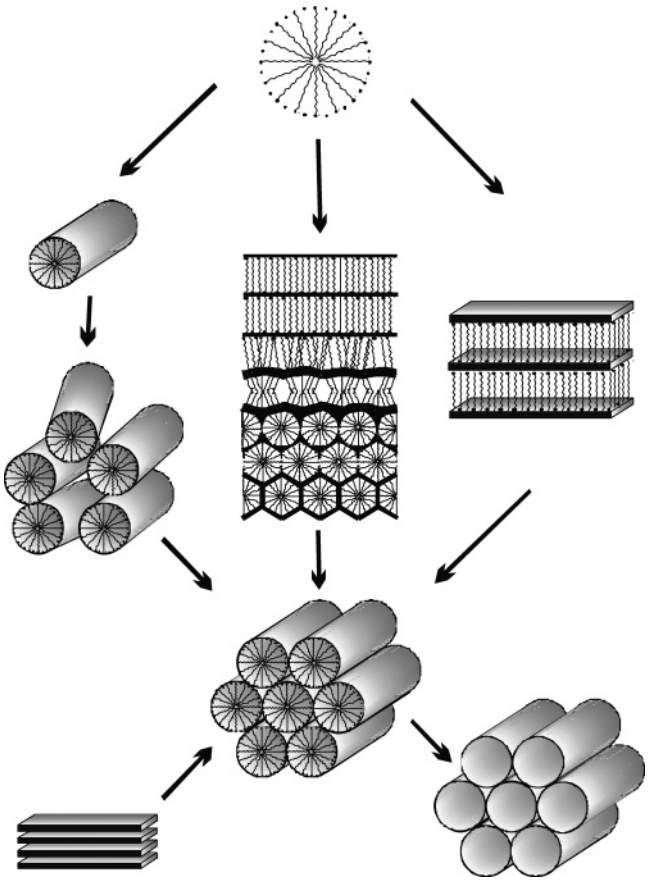

**Figure 1.** General pathway for the formation of ordered mesoporous materials.

temperature, or postsynthetic treatments.[18,27] MCM-48 is a cubic phase with $Ia\bar{3}d$ symmetry consisting of an enatiomeric pair of nonintersecting three-dimensional channel systems that are mutually intertwined. MCM-50 and the cubic octamer are in unstable phases, which collapse during template removal.

Huo et al. have synthesized a novel mesoporous molecular sieve with a three-dimensional cubic structure in highly acidic media.[30] The material is denoted SBA-1 (Santa Barbara Material No. 1) and possesses a cage-type structure with open windows. Highly ordered large pore mesoporous silicas SBA-15 with thick pore walls (ca. 3 nm) and a two-dimensional channel structure consisting of a hexagonal array of mesopores with diameters between 8 and 30 nm interconnected by micropores have been synthesized in 1998.[19,20] The relatively cheap amphiphilic triblock copolymer $EO_{20}PO_{70}EO_{20}$ (poly(ethylene oxide)-*block*-polypropylene oxide-*block*-poly(ethylene oxide), trade name Pluronic 123) is employed as the structure-directing agent in highly acidic media. The pore diameter can be tuned from 8 to 30 nm by appropriate choice of template, synthesis temperature, and swelling agent.

Tanev et al. have prepared HMS silica (hexagonal mesoporous silica) via a neutral templating route ($S_0I_0$) using neutral amines as templates ($S_0$) and neutral silica species ($I_0$).[31] Bagshaw et al.[32] reported the synthesis of a disordered mesoporous material designated MSU-1 (Michigan State University) by using poly(ethylene oxide) (PEO) as a structure directing agent. However, MSU-1 materials have up until now not been employed as supports for biomolecules and are therefore not discussed here.

Recently, Stucky and co-workers reported the preparation of MCF (mesostructured cellular foam) type materials employing triblock copolymers stabilized by oil in water microemulsions.[33] These materials possess three-dimensional, continuous, ultra-large pore mesoporous structures with large spherical cells interconnected by uniform windows. The diameter of the windows (9−22 nm) and of the spherical cells (24−42 nm) can be tuned by adjusting the amount of swelling agents and the synthesis temperature. These materials resemble aerogels but offer the additional benefit of a facile synthesis in combination with well-defined pores.

A rather new development is the synthesis of chiral mesoporous silica by Che et al.[34] Transmission electron microscopy together with computer simulations of the novel materials confirm the presence of hexagonally ordered chiral channels with a diameter of 2.2 nm winding around the central axis of the rods. However, the pitch is at present too long to induce chirality in order to synthesize enantiomerically pure chemicals.

The ordered mesoporous materials described above were used as templates for the preparation of ordered mesoporous carbons. This work was pioneered by the group of Ryoo (CMK-x materials); independently and somewhat later, similar approaches were published by Hyeon and co-workers (the materials were denoted SNU-x).[35] The principle procedure is represented in Figure 2. An ordered mesoporous silica is impregnated with a precursor for carbon such as sucrose,[36] furfuryl alcohol,[37] resorcinol-formaldehyde,[38] or vinylbenzene.[39] In the first report on this topic, the ordered mesoporous carbon CMK-1 (Carbon Molecular Sieve Korean Advanced Institute of Science and Technology No. 1) was prepared using MCM-48 as a template and sucrose as the carbon source.[36] The first ordered mesoporous carbon that was a faithful replica of the template was synthesized employing SBA-15 as a template.[40] The material consists

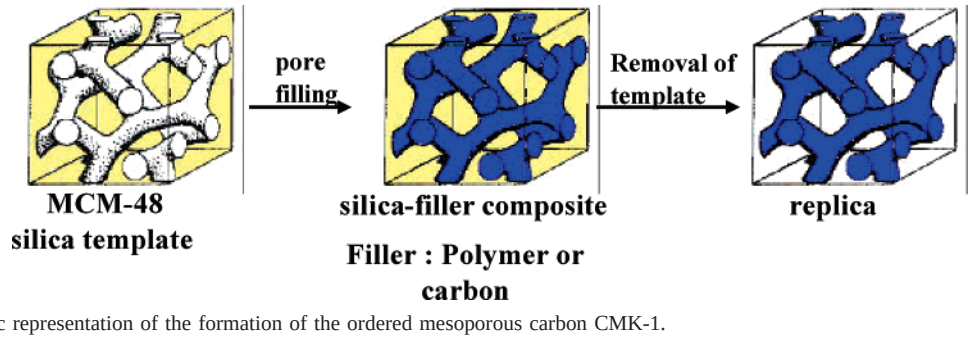


**Figure 2.** Schematic representation of the formation of the ordered mesoporous carbon CMK-1.

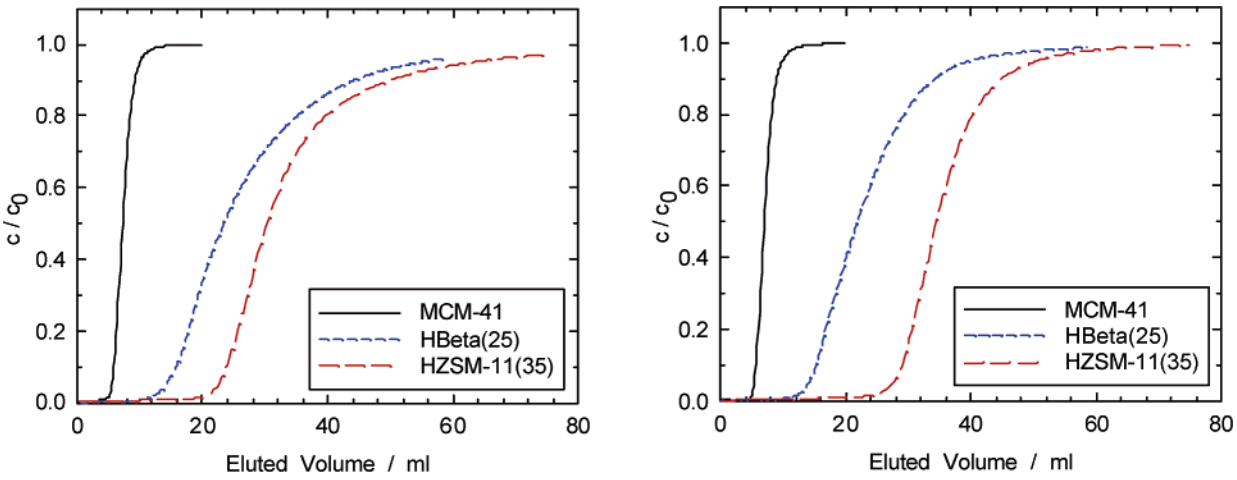


**Figure 3.** Breakthrough curves of (a) phenylalanine and (b) leucine on MCM-41, zeolite Beta ($n_{Si}/n_{Al} = 25$) or ZSM-11 ($n_{Si}/n_{Al} = 35$) as adsorbents. Reproduced with permission from ref 45.

of uniformly sized carbon rods arranged in a hexagonal pattern. At first sight, it was rather surprising that SBA-15 leads to the stable carbon replica CMK-3. Unconnected channels should not lead to the formation of a free-standing 3D structure but rather to disconnected carbon rods. However, there is growing evidence since the discovery of SBA-15 that there are micropores connecting the mesoporous channels.[41−43] Since the connecting micropores are also filled with carbon precursor, they form structure-supporting links between the carbon rods.

### 3. Adsorption of Small Biological Molecules

Amino acids are used on a large scale as supplement to stock feed and for the improvement of proteins in food technology. In this context, mesoporous silicas have been tested as adsorbents for the adsorption of amino acids from aqueous solution.[44] The adsorption of various amino acids from aqueous solution using MCM-41-type mesoporous molecular sieves was studied by Ernst et al.[44] The achieved adsorbent loadings strongly depend on the pH and the nature of the individual amino acid: Acidic amino acids (e.g., glutamic acid) are hardly adsorbed, whereas basic amino acids (i.e., lysine) show very high affinities to the mesoporous adsorbent. The uptake of amino acids with nonpolar side chains increase with chain length. The adsorption complex is proposed to consist of the cationic form of the amino acid attached to the negatively charged silica surface. Moreover, these electrostatic interactions are complemented by hydrophobic interactions probably between neighboring adsorbate molecules.[44]

The continuous adsorption of phenylalanine and leucine on $C_{14}$−MCM-41 was studied on MCM-41 in comparison to the microporous zeolites HBeta and HZSM-11. The breakthrough curves (parts a and b of Figure 3) display the typical behavior found in a fixed-bed adsorber.[45] In the beginning of the adsorption experiments, the amino acids are fully adsorbed. After a certain eluted volume (a certain time-on stream), a sharp rise of the breakthrough curve is detected which marks the breakthrough of the amino acid. Finally, the amino acid concentration at the adsorber outlet reaches the initial amino acid concentration. Integration of the breakthrough curve allows the determination of the amount adsorbed, which amounts to 48, 439, and 338 $\mu$mol/g for MCM-41, HBeta, and HZSM-11, respectively. Thus, MCM-41 is found to be an inferior adsorbent as compared to classical zeolites.[46] However, the amino acids adsorbed on MCM-41 can be completely recovered by flushing with water, while only ca. 50 and 30% of the adsorbed amino acids can be desorbed with water from HBeta and HZSM-11, respectively.[45]

Mesoporous silica was used as a stationary phase in high-performance liquid chromatography (HPLC) for the separation of biomolecules such as cysteine, glutathione, 6-thiopurine, and dopamine.[47] SBA-15 modified with dimethyloctadecylclorosilane ($C_{18}$−SBA-15) was packed in a capillary column and used for reverse-phase chromatography with an aqueous mobile phase. The observed resolution was better than that observed for a commercial column under similar conditions. The intrinsic performance of $C_{18}$−SBA-15 as a HPLC substrate was also demonstrated in the separation of peptides obtained by digestion of myoglobin by trypsin. The molecular weights of myoglobin peptides are in the range of 280−1900 Da and the numbers of amino acids range from 2−16.

The adsorption of vitamin B2 (riboflavin) onto MCM-41 and MCM-48 was studied by Kisler et al.[48] MCM-41 shows significantly higher adsorption of vitamin B2 compared to MCM-48 (0.015 vs 0.005 $\mu$mol/g). This effect is tentatively ascribed to the difference in pore size (4.1 vs 2.1 nm) between MCM-41 and MCM-48. Adsorbed vitamin B2 has a maximum size of roughly 60% of the MCM-48 pore size, and thus steric hindrance is believed to play an important role. Desorption experiments revealed that some vitamin B2 remains adsorbed, showing that the adsorption is not completely reversible under the conditions tested. However, the adsorption capacity of mesoporous silica molecular sieves for vitamin B2 was significantly lower than that achieved with mesoporous activated carbon samples with similar surface area.[49]

Adsorption of vitamin E over mesoporous carbon materials such as CMK-1 and CMK-3 has been studied from vitamin E solutions in *n*-heptane and *n*-butanol, and the results are

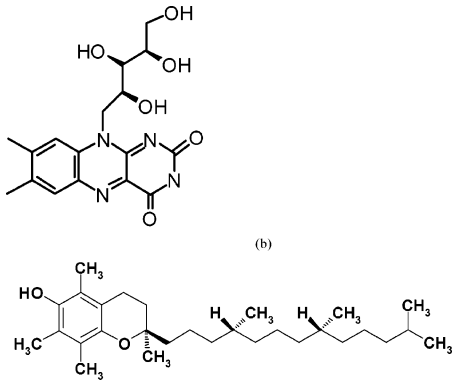


**Figure 4.** Structures of (a) vitamin B2 (riboflavin) and (b) vitamin E.

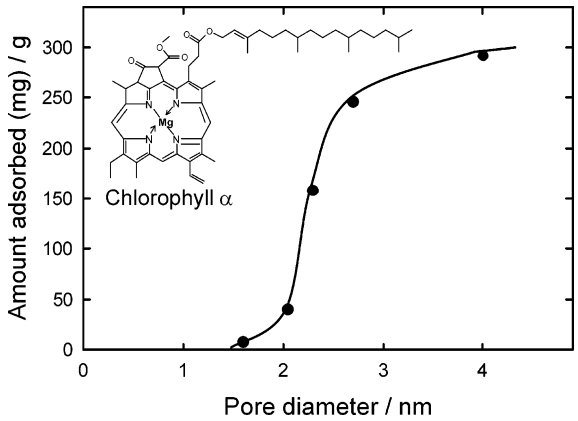


**Figure 5.** Relationship between the amount of chlorophyll adsorbed and the pore diameter of FSM-16. Reproduced with permission of the Royal Society of Chemistry from ref 51.

compared with a conventional microporous carbon adsorbent, namely, activated carbon.[50] It has been observed that the vitamin E adsorption capacity of the adsorbents depends on the solvent as well as on the mesopore volume and the pore diameter of the adsorbent. It has been found that a nonpolar sovent such as *n*-heptane is a more suitable solvent than the polar solvent *n*-butanol to achieve the maximum adsorption of vitamin E. CMK-3 exhibited the highest amount of vitamin E adsorption (5.94 mmol/g), which is significantly higher as compared to CMK-1 and activated carbon, which exhibited amounts of vitamin E adsorption of 5.01 and 4.10 mmol/g, respectively. $N_2$ adsorption and X-ray diffraction (XRD) data after vitamin E adsorption reveals that the vitamin E molecule is packed tightly inside the mesopore channels of mesoporous carbon adsorbents.

The adsorption of chlorophyll *a* extracted from natural *Spirulina* on FSM-16 was investigated by Itoh et al.[51−53] It is found that the amount adsorbed strongly depends on the pore size of the adsorbent. Silica gel and FSM-16 with pore sizes less than 2 nm adsorb very little chlorophyll, while ca. 30 wt. % was adsorbed on FSM-16 with a BJH pore diameter of 4 nm (Figure 5). The adsorption isotherms at 25 °C are of the (pseudo)Langmuir type (type L) and reach the saturation level at equilibrium concentrations exceeding 10 mmol/L. Chlorophyll adsorbed on FSM-16 was found to exhibit a higher photostability as compared to chlorophyll in benzene. An absorption maximum of 665 nm was observed for isolated chlorophyll in benzene, whereas an absorption maximum of 677 nm was found for adsorbed

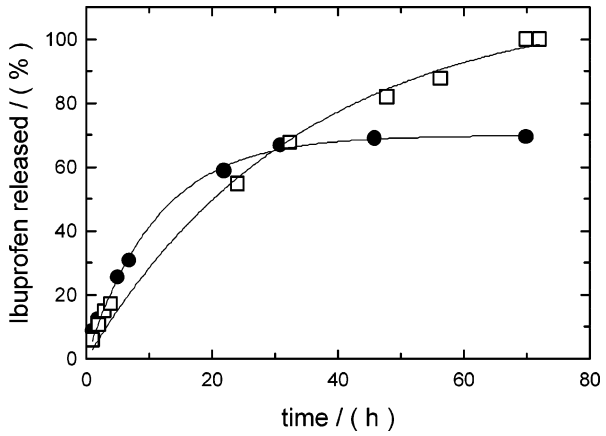


**Figure 6.** Release of ibuprofen from $C_{12}$−MCM-41: (■) Method 1; (●) Method 2. Reproduced with permission from ref 55.

chlorophyll. Chlorophyll in intact leaves exhibits an absorption maximum of 678 nm and is quite stable against light. The observed high photostability of adsorbed chlorophyll is attributed not only to its interaction with the adsorbent FSM-16 but also to chlorophyll−chlorophyll interactions in a dimer-like arrangement in the FSM-16 pores.[51] As the chemical structure of the chlorophyll *a* consists of two parts, a Mg−porphyrin head moiety and a phytol hydrophobic tail chain, both parts are expected to interact with solvents and the silica surface in a different way and are likely to control the adsorption and self-organization of chlorophylls inside the mesopores. Different types of interaction seem to occur among chlorophyll aggregates inside mesoporous silica with suitable pore size resulting in efficient stable photochemical activity. The surface properties of silica seem also to be important to achieve high adsorption and well-organized molecular interaction.[53]

Dextrans, a family of polysaccharide molecules, have been used to develop model adsorption systems using relatively simple (and stable) molecules as compared with other biomolecules such as proteins. The adsorption of dextrans with different molecular weight on SBA-15 and MCF molecular sieves has been studied by Yiu et al.[54] The amount of dextrans adsorbed decreases with increasing molecular weight between 10 and 40 kDa. Dextrans with a molecular weight of 68 kDa were not adsorbed on SBA-15, because the molecules are too large to fit into the SBA-15 pores. MCF were, however, able to adsorb the largest dextran studied.

MCM-41 was tested as drug delivery system for the controlled release of ibuprofen (size = 1.0 × 0.6 nm), an anti-inflammatory drug.[55] A maximum uptake of 0.3 g of ibuprofen per g of $C_{12}$−MCM-41 was observed. Thereafter, the drug-charged material was shaped into disks to improve the drug-release process (Method 1). The release curve was obtained by immersing the sample into a defined volume of simulated body fluid (SBF). Figure 6 shows that the initial release is fast, reaching 60% after 24 h, and reaches a maximum value of 70% after 32 h. If ibuprofen is loaded into MCM-41 after disk formation (a $C_{12}$−MCM-41 wafer is immersed into the ibuprofen solution in *n*-hexane, Method 2), the delivery rate is almost similar, but the release reached 100% of the ibuprofen adsorbed. This preliminary study

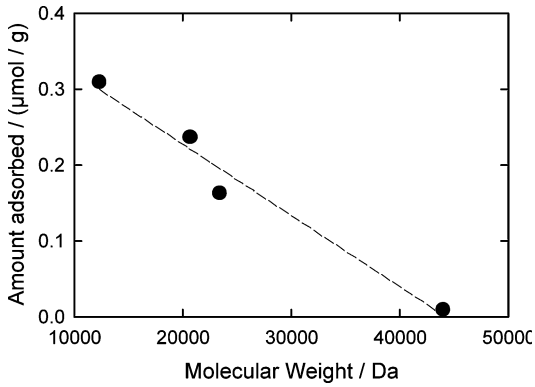


**Figure 7.** Effect of enzyme size on the immobilization efficiency of MCM-41 as support. Reproduced with permission from Elsevier from ref 58.

demonstrates the feasibility of designing drug-release systems by suitable choice of the support and the drug. However, Method 2 is preferred since loading after shaping ensures that all of the ibuprofen can be released. For Method 1, some of the drug may be occluded in the particle, which prevents its release.

A stimuli-activated drug-release system was also reported. Fujiwara and co-workers functionalized MCM-41 with a photoactive coumarin derivative that is known to reversibly dimerize upon photo irradiation.[56,57] For effective release control, the coumarin was grafted only to the pore mouth of as-synthesized MCM-41 followed by removal of the template. Exposing this material to a solution of guests (i.e., cholestane or progesterone) induced guest inclusion in the pores. Irradiation of UV light (>310 nm) caused dimerization of the coumarin to stably store the guest. The dimerized coumarin was effectively cleaved upon irradiation of UV light at around 250 nm, and the guest molecules were released.

## 4. Immobilization of Proteins on Mesoporous Silicas and Carbons

Balkus and co-workers were the first to publish work on the immobilization of globular proteins (cytochrome *c*, papain, trypsin) on MCM-41.[58] A clear dependence of the protein size on the achieved loading was found (Figure 7). Horseradish peroxidase (HRP) was not significantly retained by MCM-41 ($d_p$ = 4 nm) indicating that the enzyme molecules (4.0 × 4.4 × 6.8 nm$^3$) were too large to fit into the MCM-41 pores.

**4.1. Cytochrome *c*.** Cytochrome *c*[59,60] is a small heme protein (MW: 12 400 Da) and consists of a single polypeptide chain of 104 amino acid residues that are covalently attached to the heme group. The active heme center consists of a porphyrin ring, where the four pyrrole nitrogens are coordinated to the central Fe atom forming a square planar complex. The iron center switches between the ferric ($Fe^{3+}$) and the ferrous ($Fe^{2+}$) state, thus acting as a one-electron carrier. Because of its outer electronic structure, $Fe^{3+}$ can exist in high-spin or low-spin states. In solution, the iron of cytochrome *c* exists in the low-spin state at pH between 2 and 12. The heme center is surrounded by tightly packed hydrophobic side chains, a polypeptide chain framework, and an outer covering of hydrophillic side groups. Only one edge

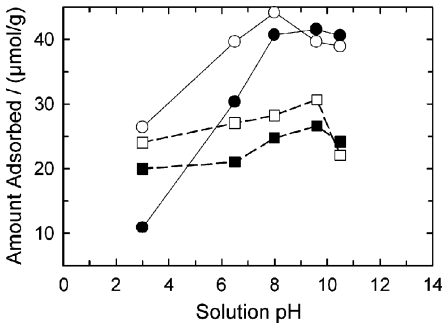


**Figure 8.** Monolayer capacities of cytochrome *c* adsorbed on (○) AlSBA-15, (●) SBA-15, (□) $C_{16}$−AlMCM-41, and (■) $C_{16}$−MCM-41 as a function of the solution pH. Reproduced from ref 68.

of the planar heme ring is accessible to the surface. The cationic side chains of several lysine residues are clustered at the surface of the molecule. Cytochrome *c* is a nearly spherical (2.6 × 3.2 × 3.0 nm$^3$) basic protein with an isoelectric point (pI) of 9.8. The pI is the pH value in solution at which the sum of the charges on the protein is zero. Some research groups have reported the adsorption of cytochrome *c* on various mesoporous molecular sieves.[58,61−67] Early studies report the adsorption of cytochrome *c* in mesoporous silica molecular sieves such as MCM-41, MCM-48, SBA-15, Nb-TMS-1 (a hexagonal niobium oxide), and Nb-TMS-4 (a layered niobium oxide). However, the uptake was only measured from low concentrated solutions, and loadings up to 11 mg/g (0.95 µmol/g) were achieved.

Deere et al.[63,64] were the first to report adsorption isotherms at 25 °C of cytochrome *c* on different mesoporous silica molecular sieves (MCM-41, MPS-127, silica (COS), and cyano-modified silica (CNS)). The isotherms were recorded at a pH of 6.5 and are of the (pseudo)Langmuir type. The capacity for cytochrome *c* increases in the order MCM-41 < COS < MPS-127 < CNS. A maximum loading of 10.2 µmol/g was achieved under the conditions employed in this study. Adsorbed cytochrome *c* was found to be stable to repeated washing in buffer (pH = 6.5) solution, which is in line with previous studies. It has previously been shown that cytochrome *c* desorbs from mesoporous materials at pH = 10, which is close to the pI of cytochrome *c*.[62] To prevent cytochrome *c* leaching a pH > 10, the effective pore aperture of MCM-48 was modified with 4-(trichlorosilyl)-butyronitrile after cytochrome *c* adsorption and the enzyme was encapsulated. Whether reducing the pore aperture by silylation is a generally applicable strategy to prevent leaching from the mesoporous, it has still to be proven. Moreover, silylation has to be performed carefully to prevent pore blocking thereby restricting or prohibiting access of the substrates or analytes to the protein.

The influence of the solution pH on the adsorption of cytochrome *c* was studied by Vinu et al.[67,68] Different mesoporous materials (MCM-41 and SBA-15) with various pore diameters have been synthesized under different conditions and characterized by X-ray powder diffraction and nitrogen adsorption measurements. Adsorption of cytochrome *c* over these adsorbents has been studied from solutions with different pH. It has been found that the amount of cytochrome *c* adsorbed on different adsorbents was significantly changed by adjusting the solution pH (Figure 8). The

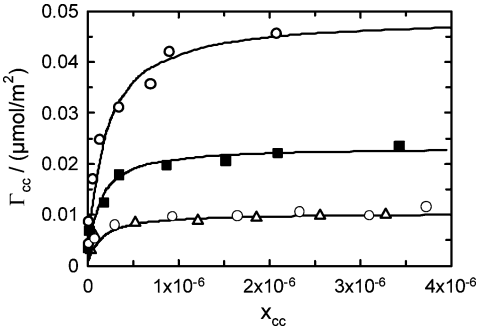


**Figure 9.** Comparison of the cytochrome *c* adsorption isotherms on mesoporous adsorbents with various pore diameters at pH 9.6: (●) SBA-15, (■) $C_{16}$−MCM-41, (▲) $C_{12}$−MCM-41, and (○) amorphous silica. Reproduced from ref 68.

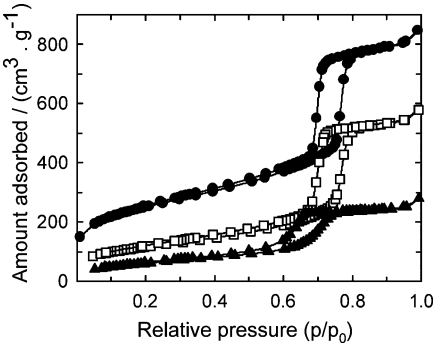


**Figure 10.** Nitrogen adsorption isotherms of SBA-15 before and after cytochrome *c* adsorption at pH 9.6: (open symbols, adsorption; closed symbols, desorption): (●) SBA-15, (□) SBA-15(1 g/L), and (▲) SBA-15(4 g/L).[68]

maximum loading of cytochrome *c* has been achieved near the pI of cytochrome *c* (9.8). This may due to the zero net charge of the cytochrome *c* molecule at this pH, and thus there is no electrostatic repulsion or attraction between the amino acid residues, resulting in a size reduction of the cytochrome *c* molecule. It has also been discovered that the amount of cytochrome *c* adsorption can be increased by the introduction of aluminum sites into the pure silica materials. The observed increase in adsorption capacity is probably a consequence of the strong electrostatic interaction between the negative charges on the aluminum sites and the positively charged amino acid residues on the surface of cytochrome *c*. The influence of pore diameter on the adsorption of cytochrome *c* has also been studied by using adsorbents with different pore diameter (Figure 9). To account for the difference in surface area, the reduced area surface excess is plotted against the molar fraction of cytochrome *c* in solution. It has been found that the amount adsorbed is mainly a function of the specific pore volume and that ca. 30% of the total pore volume is occupied by the protein assuming that the protein requires a space for adsorption that is similar to its geometrical size. Furthermore, the rate of cytochrome *c* adsorption on the powder and the pellet form of the adsorbent has been studied. While the adsorption capacity is reduced upon bead formation (due to the reduction in specific pore volume), the rate of adsorption is mainly unchanged. The study of the adsorption kinetics reveals that 96 h are required to establish adsorption equilibrium.

Adsorption isotherms of cytochrome *c* on MCM-41 and SBA-15 at pH = 6.5 have been reported by Deere et al.[63,65,66] up to an equilibrium concentration of 10 μmol/L. At this concentration, the amount adsorbed corresponds to 1, 8, and 6.8 μmol/g for MCM-41 ($d_p$ = 2.8 nm), MCM-41 ($d_p$ = 4.5 nm), and SBA-15, respectively. This is in line with results of Vinu et al.[68] at this equilibrium concentration, although they have found that the use of higher concentrated cytochrome *c* solutions allows the adsorption of higher quantities of cytochrome *c*. This shows that Deere et al.[65] only recorded the initial part of the isotherm and that saturation was probably not reached in their experiments. The authors therefore concluded that cytochrome *c* is not entering the mesopores of MCM-41 ($d_p$ = 2.8 nm), while the data of Vinu et al. clearly show that cytochrome *c* is adsorbed in the mesopores of $C_{12}$−MCM-41, which has a pore diameter of ca. 3.0 nm (NLDFT method). Moreover the pore volume of the material used by Deere et al. is very low (0.31 cm$^3$/g for MCM-41 ($d_p$= 2.8 nm)) which also accounts for the low adsorption capacity observed. In a more recent paper of the same authors, an adsorption capacity of 8 μmol/g was found for a MCM-41 sample with a higher pore diameter ($d_p$ = 4.5 nm).[27] Balkus et al.[58,62] studied the adsorption of cytochrome *c* at 0 °C and pH = 7 onto MCM-41, MCM-48, and SBA-15. The maximum adsorption reported was around 7 μmol/g starting from solution concentrations of 15 μmol/L, which is well below the final concentration used in the studies of Vinu et al.[67,68] (ca. 320 μmol/L).

Recently, Deere et al.[65] studied the influence of ionic strength on the amount of cytochrome *c* adsorbed by adding different amounts of NaCl. Over the range of ionic strength investigated, the amount of protein adsorbed strongly decreases with increasing ionic strength of the solution. Moreover, the pI of the silica adsorbent is found to play an important role. It is suggested that the surface charge of the protein and the charge of the mesoporous adsorbent must be complementary for adsorption to occur in addition to the requirement that the pore diameter must be sufficiently large.

To answer the question whether cytochrome *c* enters the mesopores of MCM-41 and SBA-15, Vinu et al. also characterized their adsorbents by XRD and nitrogen adsorption after protein adsorption.[67,68] All samples (SBA-15 and $C_{12}$−MCM-41 are exemplarily described) exhibit XRD patterns typically observed for SBA-15 and $C_{12}$−MCM-41, respectively, consisting of a strong (100) reflection at low angle and two small peaks at higher angle. The observation of these peaks even after loading the sample at a pH of 9.6 with ca. 41.5 μmol/g cytochrome *c* confirms retention of the hexagonal mesoporous structure. $N_2$ adsorption isotherms of SBA-15 and $C_{12}$−MCM-41 before and after loading with different amounts of cytochrome *c* (initial concentrations of 1 and 4 g/L) are shown in Figure 10 and Figure 11, respectively. It is observed that the amount of nitrogen adsorbed is decreasing with increasing cytochrome *c* loading. Similar results have been obtained for other adsorbents such as $C_{16}$−MCM-41 and $C_{16}$−AlMCM-41 after cytochrome *c* adsorption. The specific surface area and the specific pore volume of all the samples are reduced after cytochrome *c* adsorption as evident from Figure 11. The large reduction in the specific pore volume and the specific surface area are tentatively attributed to the tight packing of cytochrome *c*

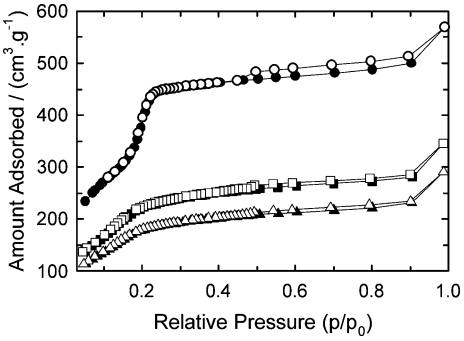


**Figure 11.** Nitrogen adsorption isotherms of $C_{12}$−MCM-41 before and after cytochrome *c* adsorption at pH 9.6: (open symbols, adsorption; closed symbols, desorption): (●) $C_{12}$−MCM-41, (□) $C_{12}$−MCM-41(1 g/L), and (▲) $C_{12}$−MCM-41(4 g/l).[68]

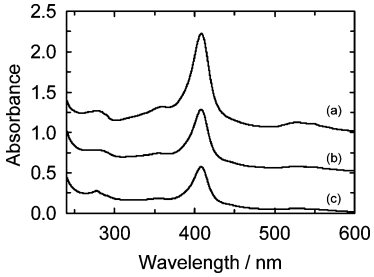


**Figure 12.** UV−vis spectra of a (a) cytochrome *c* solution ($c = 0.25$ g/L) before and after adsorption experiments with (b) $C_{16}$−AlMCM-41 and (c) $C_{16}$−MCM-41 at pH = 9.6.[68]

molecule in the pores of mesoporous materials. It is interesting to note that the reduction of the specific surface area and the pore volume of $C_{12}$−MCM-41 after different loading of cytochrome *c* adsorption is less as compared to other mesoporous materials. This shows that part of the $C_{12}$−MCM-41 pores are too small to be accessible for cytochrome *c*.

It is of fundamental importance to study not only the molecular sieve but also the adsorbed cytochrome *c* after adsorption. UV−Vis spectra of the cytochrome *c* solution before the adsorption and the supernatant cytochrome *c* solution after adsorption experiments with $C_{16}$−MCM-41 and $C_{16}$−AlMCM for 72 h are shown in Figure 12. All three spectra show a maximum at ca. 409 nm (Soret band). Moreover, it should be noted that the intensity ratio of the Soret band and the band at 365 nm is not changing during the adsorption experiments indicating that unfolding of the protein does not occur. However, in the UV−Vis DRS spectrum of cyt c adsorbed on $C_{16}$−MCM-41 and $C_{16}$Al−MCM-41, the maximum of the Soret band is shifted to ca. 406 nm and the peaks are somewhat broader compared to the liquid samples (not shown). The stability of cytochrome *c* during the adsorption was also confirmed by Raman spectroscopy in the paper by Deere et al.[65]

Cytochrome *c* is present in all organisms possessing mitochondrial respiratory chains where it serves as an electron carrier. The active site is an iron porphyrin, and the Fe(II)/Fe(III) redox couple can be conveniently characterized by electrochemical methods such as cyclic voltammetry (CV). The CV of cytochrome *c* in solution in the presence of 4,4′-bipyridyl or its derivatives as a diffusible electron-transfer mediator has been intensively studied. The CV of immobilized cytochrome *c* confirmed that the protein retains

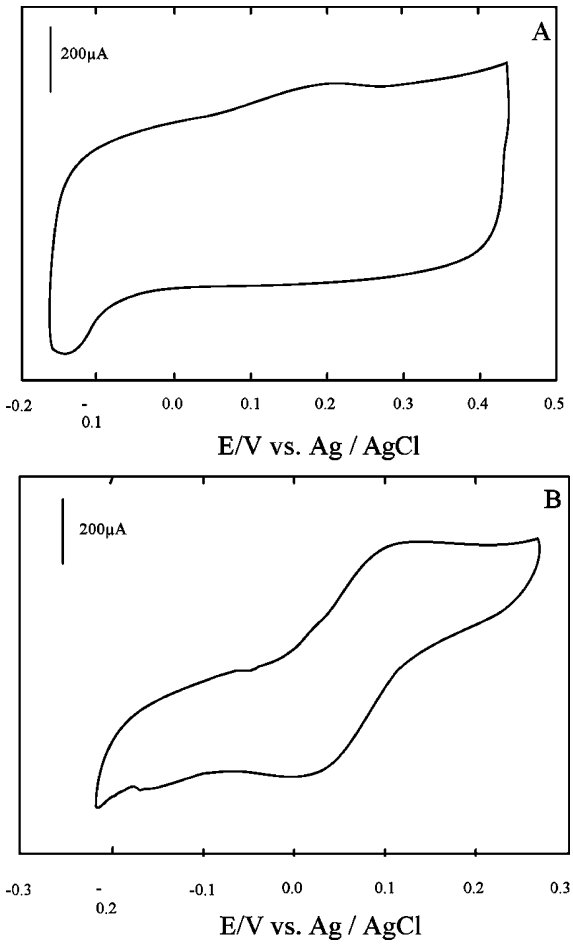


**Figure 13.** Cyclic voltammograms for cytochrome *c* (a) immobilized on MCM-48 and (b) in solution ($c = 100$ μmol/L). Reproduced with permission from Elsevier from ref 62.

activity and selectivity upon immobilization.[61,62] However, the shift of the observed redox potential for immobilized cytochrome *c* relative to the enzyme in solution is related to the interaction of cytochrome *c* with the molecular sieve (Figure 13).

Cyctochrome *c* has been intensively studied using resonance Raman spectroscopy.[69] This spectroscopy is a more informative structural probe for heme proteins than Fourier transform infrared (FT-IR) spectroscopy, as it provides detailed information (primarily regarding the protein's heme environment) not accessible by FT-IR, which is typically used to determine the global α-helical and $\beta$-sheet content of proteins (vide infra). The most prominent vibrational bands in the resonance Raman spectra (Figure 14) exited at 514 nm are a result of a vibronic coupling mechanism (B-term). These refer largely to nontotally symmetric vibrations. The spin-state marker bands $\nu_{11}$, $\nu_{19}$, and $\nu_{10}$ are the most distinct bands. In the spectra of the adsorbed cytochrome *c*, next to the above-mentioned bands, the $\nu_4$ band is also quite prominent. The spin marker bands $\nu_{10}$, $\nu_{11}$, and $\nu_{19}$ indicate that the Fe heme of adsorbed cytochrome *c* exits in both the high-spin ($S = {}^5/_2$) and the low-spin state ($S = {}^1/_2$). At room temperature, aqueous cytochrome *c* is largely in the low-spin state.[70] The unexpected prominence of the depolarized $\nu_4$ band in all spectra has also been attributed to the depopulation of the low-spin state in favor of the high-spin

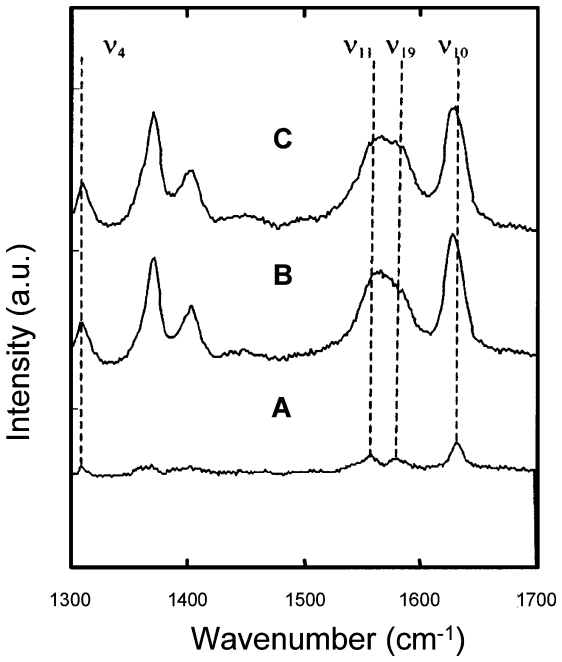


**Figure 14.** Resonance Raman Spectra of aqueous cytochrome *c* (A, 1 mM) and of cytochrome *c* adsorbed onto COS (B, 2.3 $\mu$mol/g) and CNS (C, 1.4 $\mu$mol/g). Reproduced from ref 65.

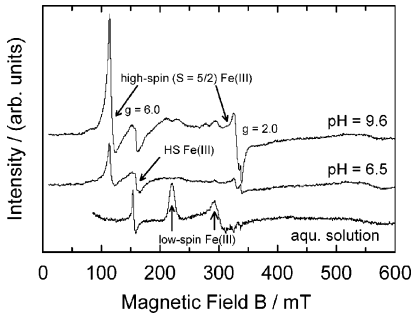


**Figure 15.** ESR spectra at 11 K of cytochrome *c* adsorbed on MCM-41 at different pHs in comparison to an aqueous solution of cytochrome *c* at a pH of 6.5.

state.[71] It is proposed that the increased activity of cytochrome *c* adsorbed on MCM-41 as compared to the free enzyme may be a result of these significantly higher levels of high spin Fe(III).

Similar conclusions are drawn from X-band electron spin resonance (ESR) spectra at 11 K.[72] Figure 15 shows the ESR spectra of cytochrome *c* adsorbed on MCM-41 at pH = 9.6 and 10.5 in comparison to the ESR spectrum of an aqueous cytochrome *c* solution. The *g* factors obtained for the aqueous solution of cytochrome *c* are in close agreement with the literature ($g_x = 1.25$, $g_y = 2.25$, and $g_z = 3.04$) and are indicative of a low-spin Fe(III) species. Two species of bound cytochrome *c* are detected: a high-spin state ($S = {}^5/_2$) with rhombic symmetry ($g = 6.0$, 5.7, and 2.0) and a high-spin state with axial symmetry ($g = 4.25$). Similar alterations of the crystal field symmetry and spin state of $Fe^{3+}$ have been reported for cytochrome *c* bound to membranes.[73]

Adsorption isotherms of cytochrome *c* on mesoporous carbon materials (CMK-3) were also investigated recently and they also showed (pseudo)Langmuir-type behavior.[74] However, the amount adsorbed is somewhat lower and significantly depends on the pH of the solution. The maximum of adsorption is close to the pI of the enzyme, which was similarly observed for the adsorption of cyt c on silica mesoporous molecular sieves. Overall charge neutralization leads to an effective adsorption of cytochrome *c* on mesoporous materials. Moreover, the effect of volume on cytochrome *c* adsorption is clearly confirmed. The adsorption capacity of mesoporous carbon materials is, however, lower compared to the silica parent material.

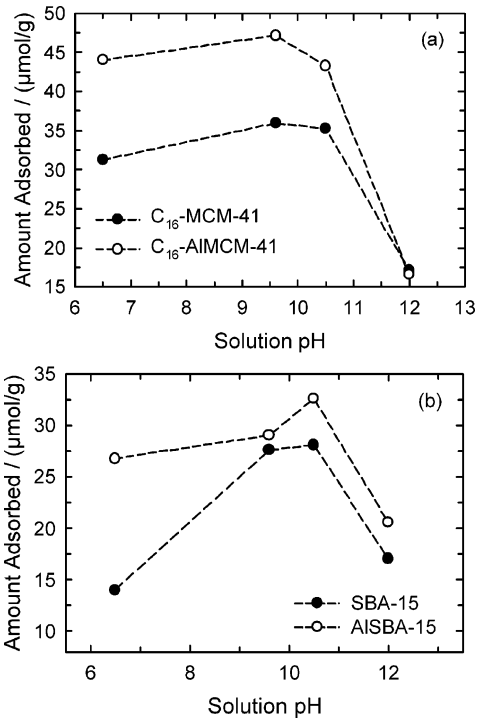


**Figure 16.** Comparison of the maximum amount of Lz adsorbed as a function of solution pH on (a) $C_{16}$−MCM-41 and $C_{16}$−AlMCM-41 and (b) SBA-15 and AlSBA-15.[87]

The adsorption of cytochrome *c* onto the external surface of a thin-film mesoporous silicate was recently studied by ellipsometry.[75] A stable film of 6−10 layers (thickness of ca. 45 nm) of protein was obtained in reasonable agreement with the number of layers (5−6) estimated from resonance Raman data.[65]

**4.2. Lysozyme.** The protein hen egg white lysozyme (Lz) has received particular attention in adsorption studies because of its well-understood structural characteristics and high stability.[76] Lz is an antimicrobial protein that is prevalent in ocular fluid; thus the adsorption of Lz on contact lenses is a considerable problem in ophthalmology.[77] It is a small globular protein (molecular mass 14 400 Da) with 18 cationic amino acid residues (6 lysyl including 1 N-terminal, 11 arginyl, and 1 histidyl) and 12 anionic residues (2 glutamyl, 9 aspartyl, and 1 leucyl C-terminal).[78] Lz has a prolate spheroid shape with two characteristic cross sections: a side of dimensions of roughly 3.0 × 4.5 $nm^2$ and an end of dimension of 3.0 × 3.0 $nm^2$.[79] The pI of Lz is around 11.[80] From the X-ray crystal structure studies, it can be seen that Lz is a hard protein up to ionic strengths of at least 0.4 and has both hydrophobic and hydrophilic amino acids exposed to the exterior.[80,81] It has been also reported that Lz is a rigid and stable enzyme because the four internal disulfide bonds help maintain its tertiary structure.[76] In the range of physi-

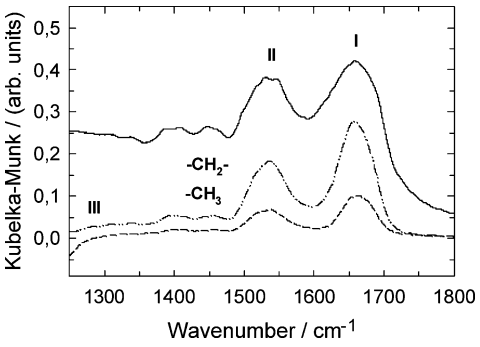


**Figure 17.** Comparison of the DRIFT spectra of pure Lz and different amount of Lz loaded on $C_{16}$−MCM-41 materials: (solid line) Lz, (dash-dotted line) $C_{16}$−MCM-41(280 $\mu$mol/L*), and (dashed line) $C_{16}$−MCM-41(69.5 $\mu$mol/L*). *Initial concentration of Lz.[87]

ological temperature, no detectable change in the structure was observed within the pH range from 1.5 to 12.

Kisler et al.[48,82] reported the adsorption of lysozyme on MCM-41 and surface-coated MCM-41. They found that the coated material shows a higher adsorption capacity as compared to the parent material MCM-41. However, it has been reported that it takes days for the adsorption of lysozyme onto these materials to reach equilibrium.[83] Zhao et al. have reported recently that, by controlling the morphology of SBA-15 type mesoporous silicas, the uptake rate and the maximum loading achieved can be drastically improved.[84,85] It has been shown that the specific capacity can reach 533 mg/g and that ca. 200 mg/g of enzyme can be completely and rapidly adsorbed with 10 min. The adsorption of lysozyme on SBA-16 and FDU 12 has been reported and it is also suggested that a large diameter of the pore entrance ($d$ > 7 nm) is beneficial for fast adsorption of the protein.[86]

Adsorption of lysozyme over mesoporous materials such as MCM-41, AlMCM-41, SBA-15, and AlSBA-15 has been studied from lysozyme solutions with different pH.[87] It has been found that the amount of lysozyme adsorbed depends on the solution pH (Figure 16) as well as the specific pore volume and the composition of the adsorbent. The maximum amount of lysozyme has been achieved for AlSBA-15 at a solution pH of 9.6, and it amounted to 47.2 $\mu$mol/g (ca. 680 mg/g). This may be due to the zero net charge of the lysozyme molecule at this pH, and so there is no electrostatic repulsion or attraction between the amino acids, resulting in a size reduction of the lysozyme molecule. By use of adsorbents with different textural properties, it has been found that the amount of Lz adsorbed is mainly a function of the specific pore volume of the adorbent. $N_2$ adsorption and XRD data after lysozyme adsorption reveal that the lysozyme molecule is adsorbed inside the channels of mesoporous adsorbents.[87] The stability toward to the buffer solution is higher for SBA-15 as compared to MCM-41, which is probably a consequence of the higher wall thickness of the former material.

To check the structural stability of Lz after adsorption on the mesoporous supports, diffuse reflectance FT (DRIFT) spectra were recorded for the Lz-loaded mesoporous adsorbents SBA-15 and $C_{16}$−MCM-41 in comparison to pure lysozyme by Vinu et al.[87] Figure 17 shows the typical DRIFT spectrum for lysozyme recorded at room temperature. There are nine normal modes that are allowed for the amide band of proteins. These are called A, B, and I−VII in order of decreasing frequency. The amide bands I−III are generally employed to study the protein structure. The amide band I (near 1650 $cm^{-1}$) is due to the C═O stretching mode, whereas the amide II band (near 1550 $cm^{-1}$) is due to the bending and the stretching mode of N−H and C−N vibrations, respectively. Typically, the disappearance of the amide II N−H stretching mode is used to follow the unfolding of the protein. The amide band III (near 1300 $cm^{-1}$) is due to the stretching and bending mode of C−N and N−H.[88] The DRIFT spectrum of lysozyme (Figure 17) shows five main bands centered at 1653, 1533, 1446, 1384, and 1252 $cm^{-1}$. It has been reported that proteins having a α-helical conformation show strong amide I bands between 1650 and 1655 $cm^{-1}$. Thus the band observed at 1653 $cm^{-1}$ is due to the α-helical confirmation of the Lz molecule. The strong amide II band at 1533 $cm^{-1}$ is due to the parallel $\beta$-sheet structure of Lz.[88] It is important to note that this band is used in assigning random structure and in accurate estimation of helix and random components.[88] The bands near 1446 and 1384 $cm^{-1}$ are assigned to the −$CH_2$− and −$CH_3$ stretching modes of the aliphatic moieties of amino acid side chains. The band at 1252 $cm^{-1}$ (amide III band) can also be assigned to $\beta$-sheets.[89] However, the amide III band is very complex and depends on the force field, the nature of the side chains, and hydrogen bonding. Therefore, this band is only of limited use for the extraction of structural information.

Figure 17 also shows the DRIFT spectrum of Lz adsorbed on $C_{16}$−MCM-41 after subtraction of the spectrum of unloaded $C_{16}$−MCM-41. The spectra also show all five major bands centered at 1653, 1533, 1446, 1384, and 1252 $cm^{-1}$. The intensities of the amide I and II bands clearly indicate that the structural confirmation of Lz is retained after adsorption on $C_{16}$−MCM-4. It can be assumed that the Lz molecules are tightly packed inside the mesopores of the material and do not have room for changing their structural confirmation inside the mesoporous matrix. Moreover, the intensities of all the five peaks in the 1700−1200 $cm^{-1}$ region rise with increasing Lz loading. This also confirms that the adsorption of Lz onto the mesoporous supports does not lead to denaturation of the protein.

The adsorption of lysozyme on ordered mesoporous carbon molecular sieves has been studied by Vinu et al.[90] Similar trends with respect to solution pH, pore volume, and pore diameter as observed for mesoporous silica molecular sieves where found for CMK-1 and CMK-3. However, the total amount adsorbed is significantly lower than observed for the silica parent materials and no benefit is gained from the additional nanocasting step required to prepare mesoporous carbons.

**4.3. HRP.** There are three classes of the plant peroxidases superfamily based on sequence alignment. Class I contains bacterial peroxidases and peroxidases from plant mitochondria and chloroplasts (e.g., cytochrome *c* peroxidase). Class II contains extracellular fungal peroxidases (e.g., lignin-degrading peroxidases), while class III contains secretory plant peroxidases. A typical member of the latter class is

the HRP isoenzyme C (HRPC). HRPC quantitatively dominates the peroxidases recovered from horseradish root. HRP has a noncovalently bound extractable heme ($Fe^{3+}$ protoporphyrin IV) center and calcium binding sites proximal and distal to the heme, four disulfide bridges, and eight N-linked carbohydrate chains. The pI of HRP is 8.8, and the molecular weight of native HPRC amounts to 44 kDa. HRP molecules possess an oval-shaped structure with an average dimension of $6.2 \times 4.3 \times 1.2$ nm$^3$, which is larger in solution due to the water layer ($6.8 \times 4.4 \times 4.0$ nm$^3$).[91] The enzymatic activity of HRP arises from the cyclic reduction and oxidation of the iron atom in the hematin group. In a suitable medium, HRP readily combines with $H_2O_2$ to form a [HRP$-H_2O_2$] complex. The complex is able to oxidize a variety of electron donors (e.g., aromatic hydrocarbons) according to the following reaction[92]

$$[\text{HRP}-\text{H}_2\text{O}_2] + \text{substrate} \rightarrow \text{product} + \text{HRP} + \text{H}_2\text{O}$$

The immobilization of HRP on different mesoporous materials has been studied by Takahashi et al.[93,94] In a typical experiment, 250 mg of the adsorbent was contacted with 5 mL of a HRP solution ($c = 10$ g/L) for 16 h at 277 K. Thereafter, the adsorbent was separated from the supernatant solution by centrifugation and washed with water. It was observed that the amount of immobilized enzyme strongly depends on the adsorbent used. A larger amount of HRP immobilization occurred on nanoporous silica templated with cationic surfactants (MCM-41 and FSM-16) as compared to materials templated with nonionic triblock copolymers (SBA-15). The authors proposed that this is due to a higher level of negatively charged groups on the surface of MCM-41 and FSM-16 and the occurrence of electrostatic interactions with the positively charged HRP (The measurements were performed at pH = 7, which is below the pI of the enzyme (8.8).) In an attempt to further investigate the electrostatic interactions, Takahashi et al.[93,94] studied the dependence of HRP immobilization on the solution pH. While no significant changes of the amount of HRP immobilized with pH was found for SBA-15 ($d_p = 5.0$ nm), the amount immobilized decreases from ca. 50 mg/g at pH = 3 to ca. 10 mg/g at pH = 9 for FSM-16 ($d_p = 5.1$ nm).

**4.4. Trypsin.** The adsorption of trypsin on mesoporous supports was studied by several groups.[48,58,82,83,95,96] Trypsin belongs to the family of enzymes known as proteases, or peptidases, which hydrolyze peptide bonds in proteins and peptides. Tryspin is a spherical protein ($3.7 \times 3.7 \times 4.2$ nm$^3$) with a molecular weight of 23.4 kDa and an pI of 10.5. Diaz et al.[58] reported an enzyme loading of ca. 4 mg/g (0.17 $\mu$mol/g) for MCM-41 at pH = 6, which was later confirmed by Kisler et al.,[48] who also found that 24−48 h are needed reach adsorption equilibrium. The latter authors also reported that loadings up to 200 mg/g (8.5 $\mu$mol/g) can be achieved when solutions with higher initial trypsin concentrations are used. Yiu et al.[95,96] reported the adsorption of trypsin on MCM-41, MCM-48, and SBA-15. Although the loadings achieved are not given, the authors report that 35−72% of the adsorbed trypsin leaches from the support after stirring in a buffer solution for 2 h. However, the immobilized enzyme is active in the hydrolysis of BAPNA (vide infra).

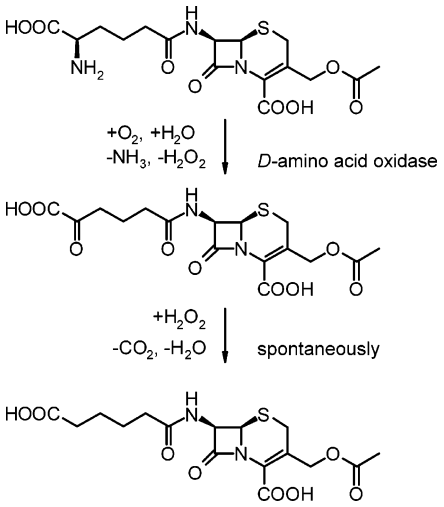


**Figure 18.** Conversion of cephalosporin C to GL-7-ACA.

**4.5. Miscellaneous Proteins and Comparison of the Adsorption of Different-Sized Proteins.** The adsorption of papain (from papaya latex) on MCM-4 was studied by Diaz et al.[58] Papain (papaya peptidase) is a thiol hydrolase of industrial importance as a meat tenderizer, an agent to remove protein cloudiness in beer, and for the production of peptones. Papain possesses an ellipsoidal shape ($3.7 \times 3.7 \times 5.0$ nm$^3$) and an pI of 8.8. The immobilization of papain is favored at low pH values (6.0 and 7.4), while at a pH of 9, which is above the pI of papain, a significantly lower loading was achieved. At this pH, it is observed that ca. 70% of the adsorbed protein leaks into solution during 24 h, while a leakage of only 15% is observed at pH = 6.

The immobilization of D-amino acid oxidase was studied over various (not ordered) silicas with pore diameters between 30 and 80 nm.[97] Covalent immobilization of D-amino acid oxidase on mesoporous silica supports was achieved by silanization of the silica surface employing 3-aminopropyl triethoxysilane (APTS), subsequent reaction with glutaraldehyde, and finally anchoring of the protein. D-Amino acid oxidase catalyzes the conversion of cephalosporin C to GL-7-ACA, which is an intermediate for the synthesis of cephalosporin antibiotics (Figure 18). The activity of immobilized D-amino acid oxidase rises with increasing pore diameter up to 45 nm but decreases thereafter. This is ascribed to leaching of the enzyme from the support during the reaction.

A similar strategy has been employed to immobilize α-amylase, which is used for the hydrolysis of starch, on SBA-15.[98] It is however found that the enzyme is immobilized only on the external surface of SBA-15. Lei et al. reported the immobilization of organophosphorus hydrolase (OPH) on surface-functionalized SBA-15.[99] Positively charged OPH is more likely to be entrapped in a material functionalized with carboxylic groups than those modified with amine groups. A higher specific activity in the hydrolysis of paraoxon was observed for immobilized OPH (4182 units/mg) as compared to the free enzyme (1928 units/mg).

The adsorption of lipase onto MCM-41 was investigated by Macario et al.[100] Lipase is a nearly spherical molecule with a diameter of ca. 4.1 nm. The adsorption kinetics of lipase onto MCM-41 have been studied at 273, 298, and 313

K. The time needed to reach equilibrium is almost independent from the adsorption temperature and amounts to ca. 18 h. The amount of lipase adsorbed decreases with increasing adsorption temperature and reaches 472 mg/g at 273 K. The activity of the immobilized enzyme was tested in the hydrolysis of triglycerides contained in olive oil into fatty acids. The activity of the immobilized lipase reaches almost 78% of the free enzyme, which is higher compared to other supports.[101,102] However, the enzymatic catalyst loses up to 50% of its activity in the fourth cycle.

The effect of pH on the adsorption of chloroperoxidase (CPO) on MCF was studied by Han et al.[103] The pI of CPO (MW = 44 kDa) is ca. 4, and thus, maximum adsorption is expected at pH values slightly below the pI. At this pH, the overall net charge of the protein is slightly positive, while the adsorbent MCF has a slightly negative charge (the point of zero charge of $SiO_2$ is ca. 2). Therefore, an electrostatic interaction between the enzyme and the adsorbent is expected. When the pH of the adsorption solution is increased to 4.3, less CPO is adsorbed. At pH = 5.5, i.e., above the pI of CPO, chloroperoxidase is not adsorbed, which is likely a result of the negative charge of both the mesoporous silica and the CPO. To determine the loading capacity of MCF (pore size = 15 nm), the adsorption of conalbumin was investigated. Conalbumin is a good model protein for CPO since it has a similar pI and comparable size and molecular weight. The loading capacity of MCF ($d_p$ = 15 nm) was found to be 122 mg of protein per gram of adsorbent, which is similar to the numbers obtained by Takahashi et al.[93,94] with MCM-41 and HRP, which has a similar molecular weight and size.

The adsorption of bovine serum albumin on Al−MCM-41 adsorbents with different aluminum content was reported.[104] Bovine serum albumin is a fairly large (MW = 66 400 Da) ellipsoidal ($4 \times 4 \times 14$ nm$^3$) protein, and it is highly questionable whether it can enter the pore system of MCM-41 with a pore diameter small than 4 nm. Up to 600 mg/g were found to be adsorbed on Al−MCM-41 with a Si/Al ratio of 10. The adsorption capacity, however, was believed to be largely due to the external surface area (278 m$^2$/g).

The adsorption isotherms at 37 °C of different proteins (i.e., cytochrome *c*, lysozyme, myoglobin, $\beta$-lactoglobulin, ovalbumin, bovine serum albumin, and conalbumin) on SBA-15 and thiol-functionalized SBA-15 were compared.[105] With the exception of ovalbumin, a higher adsorption was observed for the functionalized SBA-15 as compared to the parent material. SBA-15-based adsorbents functionalized with propylthiol groups were found to show strong and size-selective adsorption of proteins excluding those with molecular weights above ca. 44 000 such as bovine serum albumin and conalbumin (ovotransferrin).[105] The adsorption process of the smaller proteins (e.g., myglobin, $\beta$-lactoglobulin, and ovalbumin) is found to be largely irreversible indicating a strong interaction between the functionalized surface and the protein. The authors proposed that a (reversible) physisorption process is followed by a slower chemisorption. It is suggested that stacking of protein molecules with radii larger than one-half of the pore diameter of the mesoporous adsorbent is only possible one molecule at a time (analogous to single file diffusion).[105]

Han et al. investigated the size exclusion properties of SBA-15 ($d_p$ = 5.9) and MCF ($d_p$ = 16 nm) modified with APTS.[106] From a mixture with three proteins of varying size but with similar pIs (i.e., conalbumin, chicken egg ovalbumin, and soybean trypsin inhibitor protein (MW = 14 000, pI = 5.2)), APTS-modified SBA-15 sequestered and released only the small trypsin inhibitor protein, while APTS-modified MCF sequestered and released all three proteins.

The adsorption of enzymes of different sizes and pI values on MCM-41 materials with different pore diameter (i.e., 2.8 and 4.5 nm) was also reported by Deere et al.[66] The relative large proteins glucose oxidase and HRP do not adsorb on both materials, while the smaller enzymes myglobin, cyctochrome *c*, and trypsin are adsorbed on MCM-41 ($d_p$ = 4.5 nm).

In a recent study by Ravindra et al.,[107] it is shown by pressure perturbation and differential scanning calorimetry that the stability of the protein RNase A confined in the pores of MCM-48 is drastically enhanced, i.e., the temperature of thermal enfolding $T_m$ is increased by 30 °C. The increase in stability is probably not only due to a restriction in conformational space (excluded volume effect) but may also be due to an increased strength of the protein in the narrow pores of MCM-48. The latter effect certainly strongly depends on the surface chemistry of the ordered mesoporous support and may be induced by the particular water structuring properties of the silanol groups at the silica surface which are in close proximity to the protein surface when the size of the protein and the pore diameter are similar. The stabilizing effect experienced by the protein is clearly an advantage of its immobilization on the mesoporous support and is expected to be exploited in further studies.

**4.6. Whole Cells.** Another common way of utilizing enzymes is through whole-cell extracts rather than the purified enzyme. The physical immobilization of whole microbial cells of *Arthrobacter sp.*, *Bacillus subtilis*, and *Micrococcus luteus* on the mesoporous molecular sieve MCM-41 was studied by Tope et al.[108] Cells of *Arthrobacter sp.* immobilized on the matrix of MCM-41 could be successfully employed in the treatment of 2,4,6-trinitrotoluene (TNT) and its subsequent transformation to amino products. Some significant advantages observed in this novel method of immobilization were the proliferation of whole cells while on the MCM-41 matrix increase in tolerance (from 60 to 400 mg l$^{-1}$) to TNT, repeated use of the immobilized cells for 20−23 cycles, and total regeneration of the support material. However, no proof is presented that the (large) whole cells are really able to enter the pores of MCM-41.

**4.7. General Trends.** Some general trends can be deduced from the adsorption studies published so far. Adsorption is dominated by weak physical forces, i.e., van der Waals or dispersion forces. It is shown in some studies that proteins tend to adsorb better, when strong electrostatic (charge) interactions occur between the (alumino)silica surface and the protein. Near the pI, the coulomb forces derived from the positive charges from the ionized protein and the negative

charges at the silica surface are small. Under these circumstances, hydrophobic interactions between the protein and the adsorbent become more important. It is worth mentioning that hydrophobic interactions are believed to be much weaker (by about 1/13 in water) than Coulombic forces.[109] These hydrophobic interactions may either originate from attraction of the nonpolar side chains of the amino acid residues on the surface of the protein or from protein−protein interactions between the hydrophobic side chains of neighboring protein molecules. It should be noted that the surface properties of the adsorbent are of paramount importance when adsorption occurs mainly by hydrophobic interactions. More work is needed in this area to gain full understanding and control. Under the conditions of physical adsorption, the active site of the enzyme is often unaffected and nearly full activity is retained upon adsorption. However, desorption (leaching) of proteins is a common problem, in particular in the presence of strong hydrodynamic forces, since binding forces are weak.

For a given pore size of the adsorbent, smaller proteins generally adsorbed to a higher degree than larger ones, although the loading in many studies is low and far from complete filling of the mesopores. Moreover, it is unlikely that the proteins are evenly distributed in a given mesopore; they are more likely clustered at the pore entrance. For complete filling of the pore, (slow) single-file diffusion (the proteins size is often similar to the pore diameter) might hinder rapid approach to thermodynamic equilibrium. Moreover, little is known regarding the geometry of the adsorption complex on mesoporous supports. Most proteins are somewhat ellipsoidal and might adsorb with either their long and short axes with comparable probabilities. The molecule may also relax its orientation and may bind more strongly by moving its long axis from perpendicular to parallel. However, the relaxation is dependent on the surface coverage since it cannot take place if the neighboring area into which the molecule could expand is already occupied by another protein molecule. Finally, in many cases, it is furthermore found that adsorption is not completely reversible which also has a number of important implications as outlined in ref 110. In conclusion, more research work is needed to understand the fundamentals of this particular adsorption process.

In particular with respect to biocatalysis (vide infra), immobilization by cross linking or covalent anchoring is preferred. Enzymes may bind to the mesoporous support via certain functional groups such as amino, carboxyl, hydroxyl, and sulfhydryl groups. Immobilization may cause some conformational changes on the enzyme leading to denaturation. If reactive groups on the active site are involved in the covalent binding, a loss in enzyme activity can take place upon immobilization. However, in some cases, immobilization may cause an increase in enzyme activity and stability due to more favorable microenvironmental conditions.

### 5. Biocatalysis with Immobilized Proteins

HRP has been widely applied as an effective biocatalyst.[111,112] Takahashi et al.[93,94] investigated the catalytic activity of horseradish peroxidase immobilized on FSM-16, MCM-41, and SBA-15 with different pore sizes. Interestingly, pronounced differences in catalytic activity, which was assayed through oxidation of 1,2 diaminobenzene with *tert*-butylhydroperoxide, were found for HRP immobilized on different supports. HRP immobilized on FSM-16 and MCM-41 showed a higher catalytic activity as compared to HRP immobilized on SBA-15. The observed differences were explained by a better size matching between the enzyme ($4.0 \times 4.4 \times 6.8$ nm$^3$) and the pores of FSM-16 ($d_p = 5.1$ nm) and MCM-41 ($d_p = 5.0$ nm) as compared to SBA-15 ($d_p = 9.2$ nm). Moreover, FSM-16 having a pore diameter of 8.9 nm exhibits significantly lower conversion after 7 h as compared to FSM-16 with a $d_p$ of 5.1 nm.

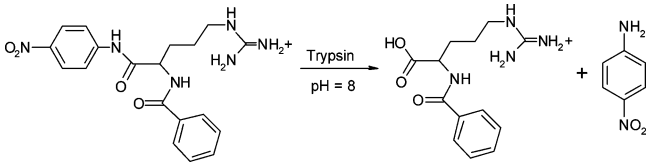


**Figure 19.** BAPNA hydrolysis by trypsin at pH = 8.

It was further shown that the thermal stability (70 °C) of immobilized HRP and subtilisin Carlsberg depends on the pore size of the adsorbent and decreases in the following order: FSM-16 ($d_p = 5.1$ nm) > FSM-16 ($d_p = 8.9$ nm) > FSM-16 ($d_p = 2.7$ nm) ≈ silica gel > native HRP. In FSM-16 ($d_p = 2.7$ nm), the enzyme is probably immobilized only on the outer surface and, therefore, a similar stability as compared to the enzyme immobilized on silica gel is very likely. A similar behavior was also found for subtilisin. The reported results show that the thermal stability is maximized when the pore diameter of the support matches the size of the enzyme.

The activity of trypsin immobilized on MCM-41 was studied at 25 °C in buffer solution at pH = 8 using the hydrolysis of *N*-α-benzoyl-DL-arginin-4-nitroaniline (BAPNA) according to the equation shown in Figure 19.[58] Assuming a similar rate for BAPNA hydrolysis for free and immobilized enzyme, the activity of immobilized trypsin corresponds to 87% of the activity found for the free enzyme. However, it was found that ca. 52% of the immobilized trypsin has leached into the solution. In subsequent experiments, the pore openings of the trypsin-loaded MCM-41 were reduced by silanation with APTS in methylene chloride at 273 K. While leaching of the enzyme could be almost completely avoided, the activity of the biocatalyst was significantly reduced. To evaluate the accessibility of the entrapped trypsin, poly-L-lysin, a known trypsin inhibitor, was added to the substrate solution. The observed results indicate that the trypsin is indeed entrapped in the pores and that obstruction of the pore openings inhibits the activity of the biocatalyst.

In contrast, Wright and co-workers claimed superiority of trypsin immobilized on SBA-15 as support compared to MCM-41 in the hydrolysis of *N*-α-benzoyl-DL-arginin-4-nitroaniline.[95,96] It was shown that the larger pore diameter of SBA-15 is advantageous in terms of substrate diffusion and pore blocking. Gomez et al.[113] studied the transesterification of *N*-acetyl-L-tyrosine ethyl ester with 1-propanol catalyzed by trypsin supported on MCM-41 (Figure 20). The adsorbed enzyme exhibited the same turnover frequency for

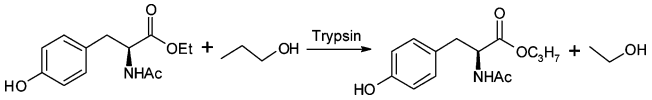


**Figure 20.** Transesterification of *N*-acetyl-L-tyrosine ethyl ester with 1-propanol.

this reaction as compared to the native enzyme. Moreover, the catalyst could be reused without loss of activity and did not leach during the catalytic testing.

Deere et al. reported that cyctochrome *c* immobilized on MCM-41 shows higher activity in ABTS (2,2′-azino (bis-(3-ethylbenzthiazoline-6-sulfonic acid) assay than the free enzyme in solution.[63,65,66] The adsorbed protein retains its peroxidative activity with no diffusional limitations being observed.[114] In aqueous buffer, the catalytic activity of the adsorbed cytochrome *c* decreases with increasing temperature. Moreover, analysis of the kinetic data by means of the Lineweaver−Burk equation and by fitting the data to the Michaelis−Menten equation showed that significant increase in the ratio $k_{cat}/k_m$ ($k_m$ is often called the Michaelis−Menten constant) occurred in methanol, ethanol, and formaldehyde primarily as a result of substantial increase in $k_{cat}$. However, it is well know that immobilized enzymes tend to exhibit elevated $k_m$ values and reduced $k_{cat}$ values owing to alterations both in partitioning and mass transport of the substrate to the immobilized enzyme. This is obviously not observed in the present system and interpreted by the authors as an increase in catalytic activity in the ABTS oxidation. Resonance Raman spectra of the immobilized cytochrome *c* revealed that the Fe(III) exits in both high- and low-spin states, while the enzyme in solution predominantly exist as low-spin Fe(III). The high-spin Fe(III) is believed to be responsible for the higher peroxidase activity of immobilized cyctochrome *c*. A similar peculiar spin state is also observed by ESR spectroscopy as shown in Figure 15.[72]

The catalytic activity of chloroperoxidase immobilized on different mesoporous silica supports was reported by Han et al.[103] The MCD assay (one unit of CPO will catalyze the conversion of 1 $\mu$mol of monochlorodimedon to dichlorodimedon per min at pH 2.75 and $T = 25$ °C in the presence of KCl and $H_2O_2$) was performed to determine the enzymatic activity of immobilized CPO. It is found that the reaction rate of the immobilized enzyme is reduced as compared to CPO in solution. However, the rate of the immobilized enzyme still shows Michaelis−Menton saturation kinetics, which indicates that immobilized CPO still reacts similarly to CPO in solution. The stability of immobilized CPO against the denaturants urea and guanidine salt was also investigated. It was, however, found that immobilization did not improve the stability of CPO against this particular denaturants. On SBA-15, immobilized CPO was also tested in the oxidation of indole.[115] It was found that is solely oxidized in the 2-position yielding 2-oxo-indole with selectivities exceeding 99%. Under conventional conditions, oxidation is preferred in the electron-rich 3 position. A major problem, however, is the deactivation of the catalyst by hydrogen peroxide.[116]

In an attempt to use manganese peroxidase (MnP) for chlorine-free pulp bioleaching, MnP from *Phanerochaete chrysosporium* has been immobilized on FSM-16 with a pore diameter of 7.0 nm.[117] This support has nearly the same pore diameter than the size of the enzyme and the immobilized MnP exhibits high thermal stability and tolerance to $H_2O_2$. MnP immobilized on FSM-16 retained more than 80% of its initial activity even after 10 days of reaction. Moreover, a two-stage reactor system is proposed, in which the $Mn^{3+}$ generation step and the pulp-bleaching step were separated (Figure 21). In the first step, the substrate solution comprising $Mn^{2+}$, $H_2O_2$, and malonic acid (as a chelating agent) was introduced in a column packed with FSM-16-supported MnP. In the next stage, the $Mn^{3+}$ malonate complex generated by the immobilized MnP was transferred into the bleaching vessel containing unbleached treated kraft pulp. By use of a two-stage reactor system, the conditions for the oxidation of $Mn^{2+}$ to $Mn^{3+}$ by MnP and the subsequent oxidation of lignin in pulp by $Mn^{3+}$ can be optimized independently.[117]

The catalytic activity of pencillin acylase on MCM-41 prepared via either direct immobilization (adsorption) or covalent coupling using glutardealdehyde was reported by He et al.[118] It was shown that direct immobilization gives higher activity in the enzymatic hydrolysis of penicillin G to produce 6-aminopenicillanic acid (6-APA) (Figure 22), which is a key raw material for the production of semisynthetic penicillins. The activity of the biocatalyst rises with increasing aluminum content of the support but decreases during repeated runs, which is probably a consequence of leaching of the immobilized enzyme.

The immobilization of α-chymotrypsin on MCM-41 with a loading of 170 mg/g is reported by Fadnavis et al.[119] A novel protocol involving adsorption of the precursor α-chymotrysinogen A and subsequent activation with trypsin has been developed to achieve high enzyme loadings. The enzyme α-chymotrypsin is a useful proteolytic enzyme for the preparation of peptides in aqueous and reverse micellar media, chiral molecules, and as a chiral stationary phase. The immobilized α-chymotrypsin on MCM-41 was reported to display comparable activity for 100 cycles in the hydrolysis of *N*-acety-L-phenylalanine methyl ester in aqueous media and is used for resolution of *N*-acetyl-DL-amino acid esters and racemic *trans*-4-methoxy-3-phenylglycidic acid methyl esters (Figure 23). Kinetic resolution of racemic glycidate esters such as **1** is an industrially important process since the optically pure (2*R*,3*S*)-*trans*-4-methoxy-3-phenylglycidic acid methyl ester (**2**) is used as an intermediate for the production of diltiazem, an important drug for the treatment of angina and hypertension, and in the synthesis of the side chain of taxol, an anticancer drug. α-Chymotrypsin immobilized on MCM-41 shows stereoselectivity toward the (2*R*,3*S*)-isomer with an enantiomeric excess of 65% at a conversion of 45%.[119] The catalyst was separated by simple filtration and reused at least five times without loss in activity.

It is reasonable to assume that immobilization of the enzyme on a suitable support is a prerequisite for the use of biocatalysts in large-scale processing. Besides achieving retention of the biocatalyst, immobilization is often employed to stabilize the enzyme as translational motion as well as volume-enhancing enfolding of enzymes is restricted. Moreover, encapsulation induces a change in the microenvironment with respect to pH or hydrophobicity. However, in

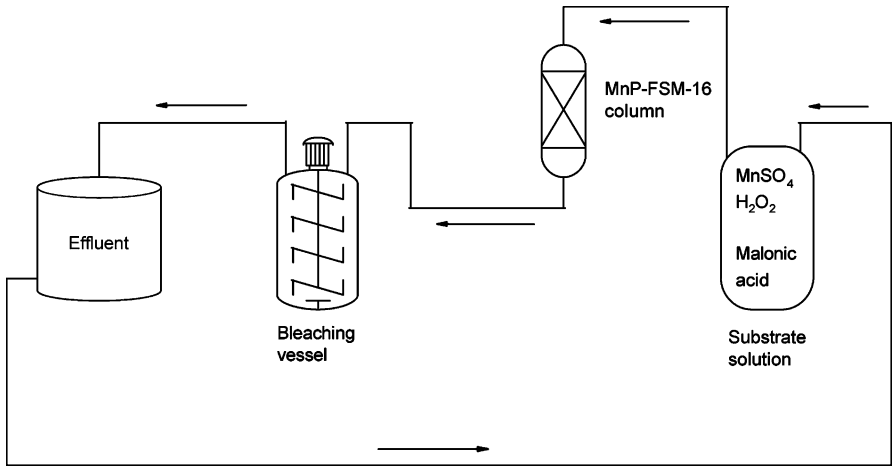


**Figure 21.** Schematic diagram of the two-stage reactor system for pulp bleaching involving MnP immobilized in FSM-16.[117]

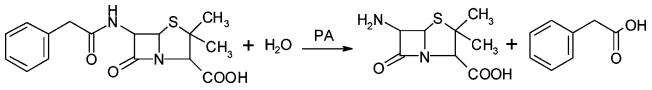


**Figure 22.** Hydrolysis of penicillin G to 6-APA.

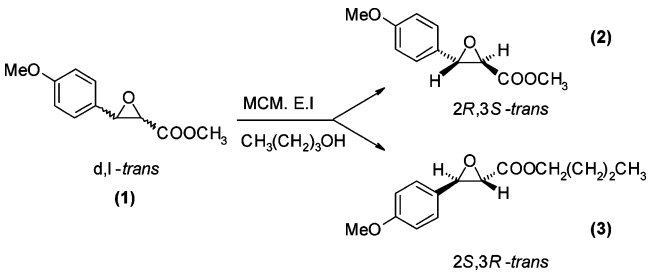


**Figure 23.** Transesterification of phenylglycidic acid methyl ester.

immobilized biocatalyst systems based on (meso)porous materials, film and pore diffusion might be rate determining instead of the catalytic reaction. It is, therefore, of uttermost importance to establish the rate-determining step under the prevailing reaction conditions. Furthermore binding to the mesoporous carrier might cause changes in the active site of the enzyme often accompanied by significant loss in catalytic activity. Even when binding does not alter the enzyme structure, some enzyme can be bound to the carrier surface with the active site oriented away from the substrate solution and toward the surface, thereby hindering access of the substrate to the active site of the enzyme.

Although many cases of successful immobilization using ordered mesoporous materials have been reported, most of the research published only uses standard activity assays to monitor the catalytic performance. There is little work up until now on the use of mesoporous support immobilized biocatalysts in real catalytic reactions. Thus, demonstration of their utility including the possibility to reuse the biocatalyst is of imminent importance. For industrial applications a major obstacle to overcome is the low space time yield in comparison to conventional (chemical) catalysts. Significant progress in this area would presumably increase the use of immobilized biocatalyst in industrial practice. Moreover, a unique feature of enzymes is their capability to catalyze reactions with high regio- and enantioselectivity. The development of novel biocatalyst would be in particular useful for the production of pharmaceuticals and fine chemicals.

Many of the enzymes (e.g., lysozyme, papain, subtilisin Carlsberg, and trypsin) investigated so far are proteolytic enzymes that have large potential in the area of proteonomics owing to their potential to produce characteristic peptides that allow peptide mass fingerprinting. In particular trypsin is one of the three principal digestive proteinases, the other two being pepsin and chymotrypsin. In the digestive process, trypsin acts with the other proteinases to break down dietary protein molecules to their component peptides and amino acids. Trypsin is the most discriminating of all the proteolytic enzymes in terms of the restricted number of chemical bonds that it will attack. Good use of this fact has been made by chemists interested in the determination of the amino acid sequence of proteins; trypsin is widely employed as a reagent for the orderly and unambiguous cleavage of such molecules. At present there is a complete lack of studies on the ability of immobilized proteolytic enzymes to cleave larger protein-based substrates, which provides an interesting area for future studies.

## 6. Biosensors

Highly ordered mesoporous niobium oxide films doped with cytochrome *c* were employed as a biosensor for the electrocatalysis of hydrogen peroxide, as cytochrome *c* adsorbed on an electrode surface displays a pseudoperoxidase activity due to the presence of cytochrome heme.[120] It is observed that the adsorbed protein molecules still retain their electrocatalytic activity and that the biosensor shows a 100% enhancement in sensitivity over the blank $Nb_2O_5$ electrode.

In a very recent paper by Dai et al.,[121] the immobilization of hemoglobin on a HMS-modified glassy carbon electrode was described. The interaction between hemoglobin and the mesoporous support was investigated employing UV−Vis and FT-IR spectroscopy as well as electrochemical methods. The direct electron transfer of the immobilized enzyme exhibited two couples of redox peaks that correspond to two immobilized states. The electrode reactions are characteristic for a surface-controlled process with a single-electron transfer. The immobilized hemoglobin retained its biological activity and displayed an excellent response to the reduction of both $H_2O_2$ and $NO_2^-$. Thus, based on hemoglobin immobilized on HMS two novel biosensors for $H_2O_2$ and $NO_2^-$ were developed, which can be used for the detection

in the concentration range from 0.4 to 6.0 $\mu$mol/L and 0.3 to 3.8 $\mu$mol/L, respectively.[121]

By recognition that there is a pressing demand for rugged, miniaturized and portable biosensing devices across fields as diverse as in vivo medical monitoring, disease diagnostics, (bio)process and environmental monitoring, food and drug quality control, genomics, and proteonomics; the lack of studies employing systems based on ordered mesoporous supports in these areas is astonishing. While optical detection might be advantageous with transparent polymers or sol−gel materials, it should nevertheless be feasible although mesoporous materials will exhibit significant light scattering. It is expected that more work is expanding into this exciting area.

## 7. Conclusions and Outlook

Although quite young, the field of mesoporous silicas and carbons doped with biologically interesting molecules has already exhibited its diversity and potential applications in many frontiers of modern materials science including biocatalysis, biosensing, drug release, and separation of biological molecules. It has been shown that ordered mesoporous materials are useful for stable entrapment of biofunctions and the stabilization of biological interesting molecules under severe conditions. For example, enzymes immobilized on ordered mesoporous supports often show higher stability as compared to the free enzyme. However, the activity of immobilized enzymes is often found to be lower than that of the free enzyme. Moreover, the access of a substrate to the enzyme confined in a mesoporous host might be orientation selective resulting in a unique selectivity of a reaction. While potential applications such as biosensing and drug release are only sparsely addressed, the ability of mesoporous adsorbents to separate molecules by size exclusion has been demonstrated. One of the major problems to be solved is the stability of mesoporous silicas upon prolonged exposure to aqueous solutions. Moreover, a possible reuse of these (at present, cost intensive) adsorbent/catalyst has to be investigated. For industrial applications, particle size and morphology of the mesoporous support are important which include several critical points such as mechanical stability and shaping of (macroscopic) particles with well-defined properties. Commercial issues such as cost of the adsorbent and scale up of the preparation of a biocatalyst or biosensor by immobilization of an enzyme have to be assessed in competition with existing materials. A major issue in biocatalysis is the low space time yield in comparison to conventional “chemical routes”. However, the high selectivity to the (enantiopure) target molecule might overcompensate this drawback. In conclusion, the use of ordered mesoporous materials is biocatalysis, bioadsorption and biosensing is a young and growing but still challenging field with still high demand of new and improved materials.

**Acknowledgment.** Generous funding of our work on ordered mesoporous materials by Deutsche Forschungsgemeinschaft and Fonds der Chemischen Industrie is gratefully acknowledged. Moreover, I would like to thank Prof. S. Ernst for his continuous support.

## References

(1) *Proteins at Interfaces II: Fundamentals and Applications*; Horbett, T. A., Brash, J. L., Eds.; American Chemical Society: Washington, DC, 1995.
(2) *Proteins at Interfaces: Physicochemical and Biochemical Studies;* Brash, J. L., Horbett, T. A., Eds.; American Chemical Society: Washington, DC, 1987.
(3) Andrade, J. D.; Hlady, V. *Adv. Polym. Sci.* **1986**, *79*, 1.
(4) Sandu, C.; Singh, R. K. *Food Technol.* **1991**, *45*, 84.
(5) Hubbell, J. A. *Bio/Technol.* **1995**, *13*, 565.
(6) Ishihara, K.; Oshida, H.; Endo, Y.; Ueda, T.; Watanabe, A.; Nakabayashi, N. *J. Biomed. Mater. Res.* **1992**, *26*, 1543.
(7) Feng, M.; Morales, A. B.; Beugeling, T.; Bantjes, A.; Vanderwerf, K.; Gosselink, G.; Degrooth, B.; Greve, J. *J. Colloid Interface Sci.* **1996**, *177*, 364.
(8) Klibanov, A. M. *Science* **1983**, *219*, 722.
(9) Rechnitz, G. A. *Chem. Eng. News* **1998**, *66*, 24.
(10) Martin, B. D.; Gaber, B. P.; Patterson, C. H.; Turner, D. C. *Langmuir* **1998**, *14*, 3971.
(11) Inglis, W.; Sanders, G. H.; Williamsan, P. M.; Davies, M. C.; Roberts, C. J.; Tendler, S. J. B. *Langmuir* **2001**, *17*, 7402.
(12) Dave, B. C.; Dunn, B.; Valentine, J. S.; Zink, J. I. *Anal. Chem*. **1994**, *66*, 1120A.
(13) Weetall, H. H. *Analtical Uses of Immobilized Biological Compounds for Detection, Medical and Industrial Uses*; Guilbault, G. G., Mascini, M., Eds.: D. Reidel Publishing Co.: Boston; MA, 1988; p 1.
(14) Weetall, H. H. *Appl. Biochem. Biotech.* **1993**, *41*, 157.
(15) Avnir, D.; Braun, S.; Lev, O.; Ottolenghi, M. *Chem. Mater*. **1994**, *6*, 1605.
(16) Gill, I. *Chem. Mater*. **2001**, *13*, 3404.
(17) Jin, W.; Brennan, J. D. *Anal. Chim. Acta* **2001**, *461*, 1.
(18) Kresge, C. T.; Leonowicz, M. E.; Roth, W. J.; Vartuli, J. C.; Beck, J. S. *Nature* **1992**, *359*, 710.
(19) Zhao, D.; Huo, Q.; Feng, J.; Chmelka, B. F.; Stucky, G. D. *J. Am. Chem. Soc.* **1998**, *120*, 6024.
(20) Zhao, D.; Feng, J.; Huo, Q.; Melosh, N.; Fredrikson, G.; Chmelka, B.; Stucky, G. D. *Science* **1998**, *279*, 548.
(21) Yang, P.; Zhao, D.; Margolese, D.; Chmelka, B.; Stucky, G. D. *Nature* **1998**, *396*, 152.
(22) Corma, A.; Navarro, M. T.; Pariente, J. P. *J. Chem. Soc., Chem. Commun.* **1994**, 147.
(23) Reddy, K. M.; Moudrakovski, I.; Sayari, A. *J. Chem. Soc., Chem. Commun.* **1994**, 1059.
(24) Schüth, F. *Angew. Chem., Int. Ed.* **2003**, *42*, 3604.
(25) Yanagisawa, T.; Shimizu, Z.; Kurida, K. *Bull. Chem. Soc. Jpn.* **1990**, *63*, 988.
(26) Inagaki, S.; Fukushima, Y.; Kuroda, K. *Chem. Commun.* **1993**, 680.
(27) Beck, J. S.; Vartuli, J. C.; Roth, W. J.; Leonowicz, M. E.; Kresge, C. T.; Schmitt, K. D.; Chu, C. T. W.; Olson, D. H.; Sheppard, E. W.; McCullen, B. B.; Higgins, J. B.; Schlenker, J. L. *J. Am. Chem. Soc.* **1992**, *114*, 10834.
(28) Vartuli, J. C.; Schmitt, K. D.; Kresge, C. T. *Chem. Mater*. **1994**, *6*, 2317.
(29) Dubois, M.; Gulik-Krzywicki, T. H.; Cabane, B. *Langmuir* **1993**, *9*, 673.
(30) Huo, Q.; Margolese, D. I.; Ciesla, U.; Feng, P.; Gier, T. E.; Sieger, P.; Leon, R.; Petroff, P. M.; Schüth, F.; Stucky, G. D. *Nature* **1994**, *368*, 317.
(31) Tanev, P. T.; Pinnavaia, T. J. *Science* **1995**, *267*, 865.
(32) Bagshaw, S. A.; Prouzet, E.; Pinnavaia, T. J. *Science* **1995**, *269*, 1242.
(33) Schmidt-Winkel, P.; Lukens, W. W.; Zhao, D.; Yang, P.; Chmelka, B. F.; Stucky, G. D. *J. Am. Chem. Soc.* **1999**, *121*, 254.
(34) Che, S.; Liu, Z.; Ohsuna, T.; Sakamoto, K.; Terasaki, O.; Tatsumi, T. *Nature* **2004**, *429*, 281.
(35) Lee, J.; Han, S.; Hyeon, T. *J. Mater. Chem.* **2004**, *14*, 478 and references therein.
(36) Ryoo, R.; Joo, S. H.; Jun, S. *J. Phys. Chem. B* **1999**, *103*, 7743.
(37) Kruk, M.; Jaroniec, M.; Ryoo, R.; Joo, S. H. *J. Phys. Chem. B* **2000**, *104*, 7960.
(38) Lee, J.; Yoon, S.; Heyon, T.; Oh, S. M.; Kim, K. B. *Chem. Commun.* **1999**, 2177.
(39) Yoon, S. B.; Kim, J. Y.; Yu, J. S. *Chem. Commun.* **2001**, 559.
(40) Ju, S.; Joo, S. H.; Ryoo, R.; Kruk, M.; Jaroniec, M.; Liu, Z.; Ohsuna, T.; Terasaki, O. *J. Am. Chem. Soc.* **2000**, *122*, 10712.
(41) Kruk, M.; Jaroniec, M.; Koo, C. H.; Ryoo, R. *Chem. Mater.* **2000**, *12*, 1961.
(42) Göltner, C. G.; Smarsly, B.; Berton, B.; Antonietti, M. *Chem. Mater.* **2001**, *13*, 1617.
(43) Hartmann, M.; Vinu, A. *Langmuir* **2002**, *18*, 8010.
(44) Ernst, S.; Hartmann, M.; Munsch, S. *Stud. Surf. Sci. Catal.* **2001**, *135*, 4566.
(45) Ernst, S.; Hartmann, M.; Munsch, S.; Thiel, H. In *Proceedings 14th International Zeolite Conference*; van Steen, E., et al., Eds.; Cape Town, 2004; pp 2020−2026.
(46) Munsch, S.; Hartmann, M.; Ernst, S. *Chem. Commun.* **2001**, 1978.
(47) Zhao, J.; Gao, F.; Fu, Y.; Jin, W.; Yang, P.; Zhao, D. *Chem. Commun.* **2002**, 752.
(48) Kisler, J. M.; Dähler, A.; Stevens, G. W.; O'Connor, A. J. *Microporous Mesoporous Mater.* **2001**, *44*−*45*, 769.
(49) Tamai, H.; Ikeuchi, M.; Kojima, S.; Yasuda, H. *Adv. Mater.* **1997**, *9*, 55.
(50) Vinu, A.; Chandrasekar, G.; Hartmann, M. *Chem. Mater*. **2005**, *17*, 829.

(51) Itoh, T.; Yano, K.; Inada, Y.; Fukushima, Y. *J. Mater. Chem.* **2002**, *12*, 3275.
(52) Itoh, T.; Yano, K.; Inada, Y.; Fukushima, Y. *J. Am. Chem. Soc.* **2002**, *124*, 13437.
(53) Itoh, T.; Yano, K.; Kajino, T.; Itoh, S.; Shibata, Y.; Mino, H.; Miyamoto, R.; Inada, Y.; Iwai, S.; Fukushima, Y. *J. Phys. Chem. B* **2004**, *108*, 13683.
(54) Yiu, H. H. P.; Bruce, I. J. *Stud. Surf. Sci. Catal.* **2003**, *146*, 581.
(55) Vallet-Regi, M.; Ramila, A.; del Real, R. P.; Perez-Pariente, J. *Chem. Mater.* **2001**, *13*, 308.
(56) Mal, N. K.; Fujiwara, N.; Tanaka, Y. *Nature* **2003**, *421*, 350.
(57) Mal, N. K.; Fujiwara, N.; Tanaka, Y.; Taguchi, T.; Matsukata, M. *Chem. Mater.* **2003**, *15*, 3385.
(58) Diaz, J. F.; Balkus, K. F., Jr. *J. Mol. Catal., B* **1996**, *2*, 115.
(59) Harbury, H. A.; Loach, P. A. *J. Biol. Chem.* **1960**, *235*, 3640.
(60) Senn, H.; Wüthrich, K. Q. *Rev. Biophys.* **1985**, *18*, 111.
(61) Gimon-Kinsel, M. E.; Jimenez, V. L.; Washmon, L.; Balkus, K. J., Jr. *Stud. Surf. Sci. Catal.* **1998**, *117*, 373.
(62) Washmon-Kriel, L.; Jimenez, V. L.; Balkus, K. J., Jr. *J. Mol. Catal., B* **2000**, *19*, 453.
(63) Deere, J.; Magner, E.; Wall, J. G.; Hodnett, B. K. *Chem. Commun.* **2001**, 465.
(64) Deere, J.; Magner, E.; Wall, J. G.; Hodnett, B. K. *Stud. Surf. Sci. Catal.* **2001**, *135*, 3694.
(65) Deere, J.; Magner, E.; Wall, J. G.; Hodnett, B. K. *J. Phys. Chem. B* **2002**, *106*, 7340.
(66) Deere, J.; Magner, E.; Wall, J. G.; Hodnett, B. K. *Catal. Lett.* **2003**, *85*, 19.
(67) Vinu, A.; Hartmann, M. In *Proceedings 14th International Zeolite Conference*; van Steen, E., et al., Eds.; Cape Town, 2004; pp 2987−2994.
(68) Vinu, A.; Murugesan, V.; Tangermann, O.; Hartmann, M. *Chem. Mater.* **2004**, *16*, 3056.
(69) Hildebrandt, P.; Heimburg, T.; Marsh, D.; Powell, G. L. *Biochemistry* **1990**, *29*, 1661.
(70) Ångström, J.; Moore, G. R.; Williams, R. J. *Biochim. Biophys. Acta* **1985**, *703*, 87.
(71) Hildebrandt, P.; Stockburger, M. *J. Phys. Chem.* **1986**, *90*, 6017.
(72) Hartmann, M.; Vinu, A.; Umameswari, V.; Pöppl, A., in preparation.
(73) Nantes, I. L.; Zucchi, M. R.; Nascimentos, O. R.; Faljioni-Alario, A. *J. Biol. Chem.* **2001**, *276*, 153.
(74) Vinu, A.; Streb, C.; Murugesan, V.; Hartmann, M. *J. Phys. Chem. B* **2003**, *107*, 8297.
(75) Deere, J.; Serantoni, M.; Edler, K. J.; Hodnett, B. K.; Wall, J. G.; Magner, E. *Langmuir* **2004**, *20*, 532.
(76) Blake, C. C. F.; Koenig, D. F.; Mair, G. A.; North, A. C. T.; Phillips, D. C.; Sarma, V. R. *Nature* **1965**, *206*, 757.
(77) Garrett, Q.; Garrett, R. W.; Milthorpe, B. K. *Invest. Ophth. Vis. Sci.* **1999**, *40*, 897.
(78) Canfield, R. E.; Liu, A. K. *J. Biol. Chem.* **1965**, *240*, 2000.
(79) Kharakoz, D. P.; Sarvazyan, A. P. *Biopolymers* **1993**, *33*, 11.
(80) Wilson, K. P.; Malcolm, B. A.; Matthews, B. W. *J. Biol. Chem.* **1992**, *267*, 10842.
(81) Bell, J. A.; Wilson, K. P.; Zhang, X. J.; Faber, H. R.; Nicholson, H.; Matthews, B. W. *Proteins* **1991**, *10*, 10.
(82) Kisler, J. M.; Stevens, G. W.; O'Connor, A. J. *Mater. Phys. Mech.* **2001**, *4*, 89.
(83) Yang, J.; Daehler, A.; Stevens, G. W.; O'Connor, A. J. *Stud. Surf. Sci. Catal.* **2003**, *146*. 775.
(84) Fan, J.; Lei, J.; Wang, L.; Yu, C.; Tu, B.; Zhao, D. *Chem. Commun.* **2003**, 2140.
(85) Lei, J.; Fan, J.; Yu, C.; Zhang, L.; Jiang, S.; Tu, B.; Zhao, D. *Microporous Mesoporous Mater.* **2004**, *73*, 121.
(86) Fan, J.; Yu, C.; Gao, F.; Lei, J.; Tian, B.; Wang, L.; Luo, Q.; Tu, B.; Zhou, W.; Zhao, D. *Angew. Chem., Int. Ed.* **2003**, *42*, 3146.
(87) Vinu, A.; Murugesan, V.; Hartmann, M. *J. Phys. Chem. B* **2004**, *108*, 7323.
(88) Adams, S.; Higgins, A. M.; Jones, R. A. L. *Langmuir* **2002**, *18*, 4854.
(89) Fu, F.-M.; DeOliveira, D. B.; Trumble, W. R.; Sarkar, H. K.; Singh, B. R. *Appl. Spectrosc.* **1994**, *48*, 1432.
(90) Vinu, A.; Miyahara, M.; Ariga, K. *J. Phys. Chem. B* **2005**, *109*, 6436.
(91) Wang, E.; Wang, H.; Li, Z. *Anal. Sci.* **2000**, *16*, 205.
(92) Fang, J.; Barcelona, M. J. *Chemosphere* **2003**, *50* 105.
(93) Takahashi, H.; Li, B.; Sasaki, T.; Miyazaki, C.; Kajino, T.; Inagaki, S. *Chem. Mater.* **2000**, *12*, 3001.
(94) Takahashi, H.; Li, B.; Sasaki, T.; Miyazaki, C.; Kajino, T.; Inagaki, S. *Microporous Mesoporous Mater.* **2001**, *44*−*45*, 755.
(95) Yiu, H. H. P.; Wright, P. A.; Botting, N. P. *Microporous Mesoporous Mater.* **2001**, *44*−*45*, 2001.
(96) Yiu, H. H. P.; Wright, P. A.; Botting, N. P. *J. Mol. Catal., B* **2001**, *15*, 81.
(97) Kim, J. K.; Park, J. K.; Kim, H. K. *Stud. Surf. Sci. Catal.* **2003**, *146*, 513.
(98) Mody, H. M.; Mody, K. H.; Jasra, R. V.; Shin, H. J.; Ryoo, R. *Ind. J. Chem. A* **2002**, *41*, 1795.
(99) Lei, C.; Shin, Y.; Liu, J.; Ackerman, E. J. *J. Am. Chem. Soc.* **2002**, *124*, 11242.
(100) Macario, A.; Calabro, V.; Curcio, S.; De Paola, M.; Giordano, G.; Iorio, G.; Katovic, A. *Stud. Surf. Sci. Catal.* **2003**, *142*, 1561.
(101) Knezevic, Z.; Mojovic, L.; Adnadjevic, B. *Enzyme Microbiol. Technol.* **1998**, *22*, 275.
(102) Taylor, F. In *Engineering of/with Lipase*; Malcata, F. X., Ed.; NATO ASI Series, 1996; Vol. 317, pp 455−472.
(103) Han, Y. J.; Watson, J. T.; Stucky, G. D.; Butler, A. *J. Mol. Catal., B* **2002**, *17*, 1.
(104) Ji, L.; Katiyar, A.; Pinto, N. G.; Jaroniec, M.; Smirniotis, P. G. *Microporous Mesoporous Mater.* **2004**, *75*, 221.
(105) Humphrey, H. H. P.; Botting, C. H.; Botting, N. P.; Wright, P. A. *Phys. Chem. Chem. Phys.* **2001**, *3*, 2983.
(106) Han, Y. J.; Stucky, G. D.; Butler, A. *J. Am. Chem. Soc.* **1999**, *121*, 9897.
(107) Ravindra, R.; Zhao, S.; Gies, H.; Winter, R. *J. Am. Chem. Soc.* **2004**, *126*, 12224.
(108) Tope, A. M.; Srivinas, N.; Kulkarni, S. J.; Jamil, K. *J. Mol. Catal., B* **2001**, *16*, 17.
(109) Matsuri, M.; Kiyozumi, Y.; Yamamoto, T.; Mizushia, Y.; Mizukami, F.; Sakaguchi, K. *Chem.*−*Eur. J.* **2001**, *7*, 1555.
(110) Ramsden, J. J. *Chem. Soc. Rev.* **1995**, *24*, 73.
(111) Scott, K. P. *Science* **1983**, *221*, 259.
(112) Blinovsky, A. M.; McEldoon, J. P.; Arnold, J. M.; Dordick, J. S. *Appl. Biochem. Biotechnol.* **1994**, *49*, 153.
(113) Gomez, J. M.; Deere, J.; Goradia, D.; Cooney, J.; Magner, E.; Hodnett, B. K. *Catal. Lett.* **2003**, *88*, 183.
(114) Deere, J.; Magner, E.; Wall, J. G.; Hodnett, B. K. *Biotechnol. Prog.* **2003**, *19*, 1238.
(115) Hartmann, M.; Streb, C. *Proceedings of the International Symposium on Advanced Materials and Processing*; Adhikari, B., Banerjee, H., Banthia, A. K., Basu, S., Bhargava, P., Jacob, C., Ram, S., Eds.; MSC: 2004; pp 584−591.
(116) Hartmann, M.; Streb, C. *J. Porous Mater.*, submitted.
(117) Sasaki, S.; Kalino, T.; Li, B.; Sugiyama, H.; Takahashi, H. *Appl. Environ. Microbiol.* **2001**, *67*, 2208.
(118) He, J.; Li, X.; Evans, D. G.; Duan, X.; Li, C. *J. Mol. Catal., B* **2000**, *11*, 45.
(119) Fadnavis, N. W.; Bhaskar, V.; Kantam, M. L.; Choudry, B. M. *Biotechnol. Prog.* **2003**, *19*, 346.
(120) Xu, X.; Tian, B.; Kong, J.; Zhang, S.; Liu, B.; Zhao, D. *Adv. Mater.* **2003**, *15*, 1932.
(121) Dai, Z.; Liu, S.; Ju, H.; Chen, H. *Biosens. Bioelectron.* **2004**, *19*, 861.
(122) Wang, Y.; Caruso, F. *Chem. Mater.* **2005**, *17*, 953.


CM0485658